 © 2014 Russian Academy of Sciences and Turpion Ltd

DOI 10.1070/RC2014v083n01ABEH004400

X-Ray photoelectron diffraction and photoelectron holography as methods for investigating the local atomic structure of the surface of solids

M V Kuznetsov, I I Ogorodnikov, A S Vorokh

Institute of Solid State Chemistry, Ural Branch of the Russian Academy of Sciences
ul. Pervomaiskaya 91, 620990 Ekaterinburg, Russian Federation

The state-of-the-art theory and experimental applications of X-ray photoelectron diffraction (XPD) and photoelectron holography (PH) are discussed. These methods are rapidly progressing and serve to examine the surface atomic structure of solids, including nanostructures formed on surfaces during adsorption of gases, epitaxial film growth, *etc*. The depth of analysis by these methods is several nanometres, which makes it possible to characterize the positions of atoms localized both on and beneath the surface. A remarkable feature of the XPD and PH methods is their sensitivity to the type of examined atoms and, in the case of high energy resolution, to the particular chemical form of the element under study. The data on experimental applications of XPD and PH to studies of various surface structures are analyzed and generalized.
The bibliography includes 121 references.

Contents

I. Introduction 13
II. X-Ray photoelectron diffraction 15
III. Photoelectron holography 28
IV. Conclusion 34

I. Introduction

Studies of the self-assembly of atoms on the surfaces of solids and the initial stages of phase formation belong to leading directions of modern chemistry as these processes play the fundamental role in heterogeneous catalysis, deposition of thin films and coatings, formation of surface nanostructures for electronics, photonics and so on. The apparent success of the surface studies is mainly related to the development of physical methods for analysis and theoretical approaches of modelling of surfaces. Combination of these methods makes it possible to determine the chemical composition and structure of surfaces, explore the electronic structure of solids, obtain their images with atomic resolution, manipulate single atoms and investigate processes occurring on the surface. It is generally accepted that there is no universal experimental method, and a set of complementary methods should be used in the surface studies. For example, the comprehensive information about the surface structure, composition and chemical state can be obtained using the combination of low-energy electron diffraction (LEED), Auger electron spectroscopy (AES), X-ray photoelectron spectroscopy (XPS), secondary-ion mass spectrometry (SIMS) and scanning tunnelling microscopy (STM).

X-Ray photoelectron spectroscopy takes a special place among the methods listed above as it is a potent method for chemical analysis of surfaces, which makes it possible to establish the chemical composition, to obtain information about the element oxidation states, to analyze valence electron states, *etc*. The depth of the analysis with the use of XPS is determined by the mean free path (λ) of photoelectrons in the material under investigation and is equal to several nanometres. The maximum depth (d) of the analysis can be achieved by recording the spectrum at the right angle to the surface, while recording at other angles leads to decrease in d to one or two monolayers, thus improving the sensitivity to the surface features. From the angular dependence of the XPS, one restores the profile of the element distribution over the depth. This approach is called angle-resolved X-ray photoelectron spectroscopy. Even at early stages of application of this method, it was noted that periodic structures appeared in the angular dependences of

M V Kuznetsov Doctor of Chemical Sciences, chief researcher of the ISSC UB RAS. Tel. (7-343) 362 33 56, e-mail: kuznetsov@ihim.uran.ru
I I Ogorodnikov Engineer at the same institute. Tel. (7-343) 362 33 56, e-mail: i_ogorodnikov@mail.ru
A S Vorokh Candidate of Physics and Mathematics Sciences, senior researcher of the same institute. Tel. (7-343) 362 33 56, e-mail: vorokh@ihim.uran.ru
Current research interests: surface structure of nanostructured materials, electronic spectroscopy, photoelectron diffraction, photoelectron holography, films, metal chalcogenides.

Received 14 April 2013
Uspekhi Khimii **83** (1) 13 – 37 (2014); translated by S E Boganov

the photoemission from single crystal surfaces.[1,2] This phenomenon was termed X-ray photoelectron diffraction (XPD). The first observations of the electron diffraction from single crystals using angle-resolved X-ray photoelectron spectroscopy were made in the mid-1970s.[3–7] It was suggested that XPD could be employed to analyze the structure of the local environment of atoms on the surface of solids. To date, a wealth of experience has been accumulated in both XPD experiments and theoretical modelling of photoelectron diffraction and interpretation of the experimental data (see, for instance, reviews [8,9–22]).

X-Ray photoelectron diffraction (and Auger electron diffraction) is based on the effect of elastic scattering of photoelectrons (or Auger electrons) by surface layers and can be implemented, for instance, by recording the angle dependences of X-ray photoelectron or Auger electron spectra, using energy dispersive analyzer or display-type hemispherical mirror analyzer in a narrow range of electron energy. In contrast to low-energy electron diffraction (LEED) and reflected high energy electron diffraction (RHEED), X-ray photoelectron diffraction detects photoelectrons which are emitted directly from the core levels of surface atoms. A major advantage of this method is the possibility of gaining structural information about each particular type of surface atoms and even about their chemically non-equivalent states since the intensity of scattered photoelectrons depends on the energy of core levels in atoms.

The intensity of emitted photoelectrons can be measured as a function of the emission direction $\boldsymbol{k}$ or as a function of energy $h\nu$ of incident photons. Therefore photoelectron diffraction is carried out by scanning over polar (θ) and azimuthal (φ) angles or over the energy of incident radiation. A laboratory X-ray source with constant photon energy is sufficient in the first case. This version ensuring high kinetic energy of electrons was called X-ray photoelectron diffraction. To carry out scanning over the energy of photons, synchrotron emission is required; below this method is called photoelectron diffraction (PD). It is believed that PD gives more accurate quantitative estimates of interatomic distances.[9] The version of X-ray photoelectron diffraction with scanning over angles is mainly considered in this review.

The inverse problem consisting in calculation of theoretical XPD patterns for model surface clusters and their comparison with the experimental data is solved to retrieve structural information from the experimental XPD picture. The theory underlying these calculations is well developed [19] and will not be discussed here in detail. If the surface is complex, this approach often fails as it is difficult to guess the surface cluster structure. In this case, photoelectron holography (PH), a method solving a direct problem of reconstructing atomic surface structure from XPD pattern as this is done in optics, can be highly helpful.

Photoelectron holography is a new rapidly progressing field of XPD. In 1986, it was proposed [23] to treat the XPD picture as a hologram and to use the electron-emitting atom as a source of coherent radiation. By analogy with optical holography, the XPD picture is a result of interference of the reference and object waves (the object is the atomic environment of the emitting atom). Since the electron wavelength used in holography is small as compared with the size of atomic structures, the electron hologram might provide detailed information about the atomic environment of the emitter. Photoelectron holography is not widely adopted yet; however, according to our opinion, the simultaneous use of this method and theoretical modelling of XPD may facilitate more precise determination of the geometry of the local environment of the atom chosen for structural analysis and gaining the three-dimensional image of scattering clusters. In recent years, there has been considerable progress in the development of this method.

The analysis of the number of publications devoted to X-ray photoelectron diffraction (Fig. 1) indicates that their maximum falls on the mid-1990s. Then the number of publications decreased and was stabilized at the level of ~ 40 publications per year. The maximum corresponds to the period of the development of XPD as a new phenomenon; the publications of that period are devoted to the theory of photoelectron diffraction and working out of algorithms of mathematical modelling of XPD.

At present, XPD can probably be acknowledged as a mature structural method for the study of surfaces and subsurface layers. From the experimental point of view, XPD and PH are organically integrated into the family of related techniques such as X-ray photoelectron spectroscopy and angle-resolved photoemission spectroscopy (ARPES). Together, they provide quantitative chemical information about surface layers, as well as about electronic structure of the surface. Curiously, XPD and ARPES began to be used almost simultaneously (see Fig. 1); however, the latter technique has acquired wider use at present as it makes it possible to explore the energy band structure of compounds. Indeed, the ARPES technique is highly demanded by physicists and material scientists since the possibility of experimental recording of the energy band dispersion patterns presents a significant opportunity to study the fundamental properties of new materials. However, the depth of analysis by ARPES embraces several subsurface layers only, and to make conclusions about the properties of the material in the bulk, it should be verified that the composition and structure of the surface layers correspond to those in the bulk. The XPD and PH methods are well suited for this purpose since they are based on the same principles and implemented on the same equipment as ARPES. The recent advances in the development of photo-

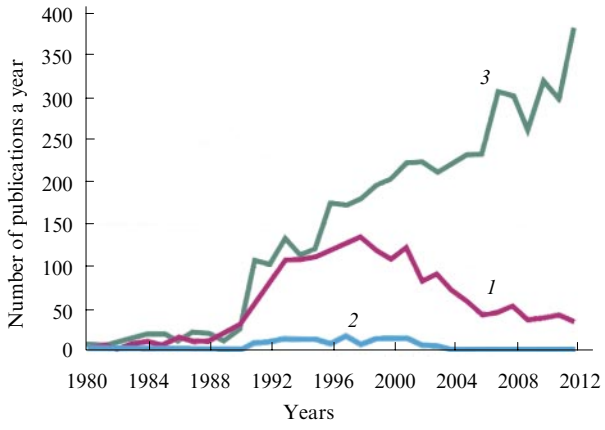


Figure 1. Dynamics of the number of publications on XPD (*1*), PH (*2*) and angle-resolved photoemission spectroscopy (*3*) according to the Web of Science database.

electron holography should increase the demand for this method from researchers engaged in the surface studies. Development of experimental technique of ARPES also facilitates wider application of XPD and PH.

What is the relationship between X-ray photoelectron diffraction and other structural methods of surface analysis? Surface images with atomic resolution can be obtained using STM, which is, perhaps, the most demanded and popular method. However, in fact, STM visualizes the density of electronic states on the surface, which is correlated with the atomic structure, but not the atomic structure itself. Only in some favourable cases, information about the second or third layer below the surface can be obtained from STM data. Therefore STM is less informative than LEED, RHEED, SIMS and X-ray photoelectron diffraction and photoelectron holography. The two last-mentioned techniques, which are discussed here, are distinguished, first of all, by variability of the depth of structural analysis ranging from surface adsorbed structures to layers that are few nanometres deep and by the fact that they provide chemical information inaccessible by other methods so far.

The goal of the present review is critical analysis of the capabilities and characteristic features of applications of X-ray photoelectron diffraction and photoelectron holography. We did not set ourselves the tasks to describe in detail the theory of photoelectron diffraction and to give various examples illustrating the use of XPD and PH, we just desired to collect and analyze the data obtained by various research groups and published in different journals. The theory of X-ray photoelectron diffraction is covered in detail in several papers.[10–19] As the examples of the use of XPD and PH, review articles devoted to these issues are published every one or two years (see, *e.g.*, Refs 9, 10, 12, 14, 15, 17, 19, and 20–22).

The general tendency in the development of XPD is obvious, it is switching from simple model objects to more complicated complex systems. Nonetheless, it is unclear yet when XPD and PH pass in their development from the stage of interesting methods with limited applicability to the level of perfect versatile approaches to surface structure analysis. Recent advances in the development of photoelectron holography (see, for example, Ref. 24) give hope for the progress along this line. We believe that the present review would be useful for researchers engaged in the fundamental and applied studies of surfaces and would present some general (although not yet completed) picture of development of XPD and PH and would prompt some ideas about promising fields of practical application of these methods.

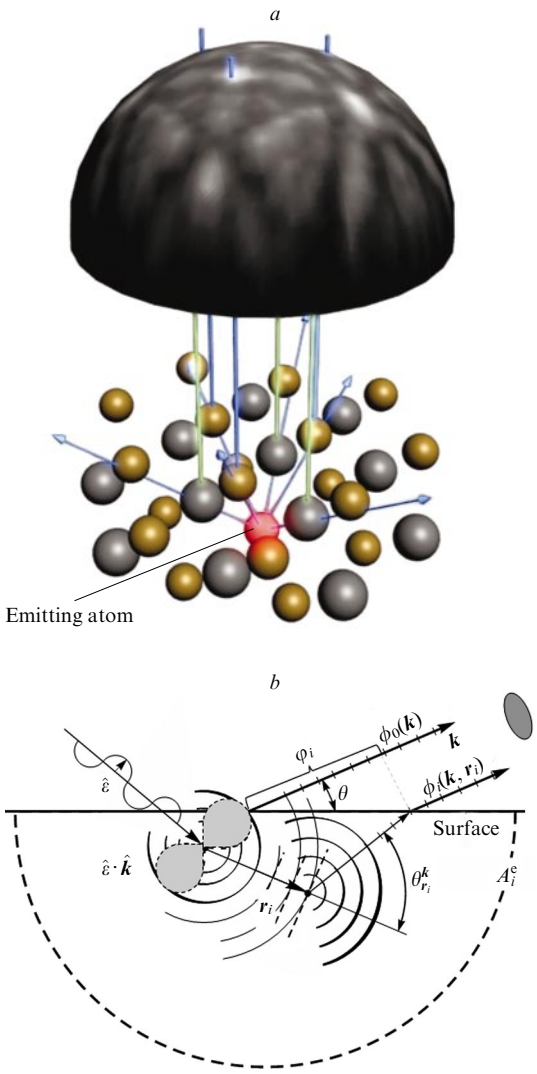


Figure 2. Major processes occurring during photoelectron diffraction (*a*) and scheme of electron single scattering in the plane-wave approximation (*b*).[15]
(*a*) The arrows indicate the directions of forward scattering and their projections on XPD 2π pattern; (*b*) designations of the variables are given in the text.

II. X-Ray photoelectron diffraction

1. Physical basis

The principal physical processes which determine the intensity of photoelectron diffraction are shown in Fig. 2. Irradiation of a surface with photons possessing certain energy results in emission of photoelectrons from the core levels of atoms. A photoelectron propagates as a spherical wave around the emitting atom and can be scattered by the nearest neighbouring atom to give a secondary wave emanating from the neighbouring atom. Both waves, namely, the direct wave from the emitting atom and the scattered wave from the neighbouring atom, which have the same wavelength and a fixed phase, add up and interfere. If atoms on the surface are arranged orderly, an interference pattern composed of all scattering events of photoelectrons with equal energy is formed in the 2π space above the sample. With the use of an electron analyzer, this interference pattern is recorded as a function of emission angle and/or electron kinetic energy. To reveal the relationship between the structural parameters and PD intensity, we consider a simple model of single scattering of a plane wave in the surface layers.[15]

The intensity of photoelectrons (I) depending on the emission direction $\boldsymbol{k}$ (electron wave vector) is determined by the interference of the unscattered wave (ϕ_0) with waves elastically scattered by ith atoms surrounding the emitting atom (ϕ_i)

$$I(\boldsymbol{k}) = \left| \phi_0(\boldsymbol{k}) + \sum_i \phi_i(\boldsymbol{k}, \boldsymbol{r}_i) \right|^2 \quad (1)$$

In the simplest case of photoemission from the s level (see Fig. 2) with the initial state s (the orbital quantum number $l_{\text{init}} = 0$) and the only final state p ($l_{\text{f}} = 1$), the dipole matrix element of photoemission is proportional to the scalar product of unit vectors of incident radiation polarization $\hat{\varepsilon}$ and the corresponding directions of injected photoelectrons:

$$\hat{\boldsymbol{k}} = \frac{\boldsymbol{k}}{k} \text{ and } \hat{\boldsymbol{r}} = \frac{\boldsymbol{r}_i}{r_i}$$

Accordingly, the unscattered wave can be expressed as

$$\phi_0 = A_0^{\text{e}}(\hat{\varepsilon} \cdot \hat{\boldsymbol{k}}) \tag{2}$$

whereas the scattered wave can be expressed in the following way:

$$\phi_i = A_i^{\text{e}} W_i \frac{(\hat{\varepsilon} \cdot \hat{\boldsymbol{r}}_i)}{r_i} f_i(\theta_{\boldsymbol{r}_i}^{\boldsymbol{k}}) \exp\left[\text{i}\left(kr_i - \boldsymbol{k}\boldsymbol{r}_i + \psi_i(\theta_{\boldsymbol{r}_i}^{\boldsymbol{k}})\right)\right] \tag{3}$$

where A_0^{e} and A_i^{e} are exponential factors for intensity attenuation due to inelastic scattering by the emitting atom and the ith scattering atom; W_i is the Debye–Waller factor allowing for the dynamic atomic displacements in solids;

$$f_i(\theta_{\boldsymbol{r}_i}^{\boldsymbol{k}}) = |f_i(\theta_{\boldsymbol{r}_i}^{\boldsymbol{k}})| \exp\left[\text{i}\psi_i(\theta_{\boldsymbol{r}_i}^{\boldsymbol{k}})\right] \tag{4}$$

$f_i(\theta_{\boldsymbol{r}_i}^{\boldsymbol{k}})$ is the complex factor for scattering of the plane wave by the ith atom of the emitter environment, $|f_i(\theta_{\boldsymbol{r}_i}^{\boldsymbol{k}})|$ and $\psi_i(\theta_{\boldsymbol{r}_i}^{\boldsymbol{k}})$ are the amplitude and phase of atomic scattering, respectively, $\theta_{\boldsymbol{r}_i}^{\boldsymbol{k}}$ is the angle between vectors $\boldsymbol{k}$ and $\boldsymbol{r}_i$.

Taking into account that

$$\boldsymbol{k}\boldsymbol{r}_i = kr_i \cos\theta_{\boldsymbol{r}_i}^{\boldsymbol{k}}$$

the phase component of the scattered wave is determined as

$$\phi_i \sim \frac{\exp\left\{\text{i}\left[kr_i(1 - \cos\theta_{\boldsymbol{r}_i}^{\boldsymbol{k}}) + \psi_i(\theta_{\boldsymbol{r}_i}^{\boldsymbol{k}})\right]\right\}}{r_i}$$

Having transformed Eqn (1), one gets

$$I(\boldsymbol{k}) = \left|\phi_0(\hat{\varepsilon} \cdot \hat{\boldsymbol{k}})\right|^2 + 2\,Re\sum_i \left[\phi_0^*(k) \cdot \phi_i(k, r_i, \theta_{\boldsymbol{r}_i}^{\boldsymbol{k}})\right] + \tag{5}$$

$$+ 2\,Re\sum_{i \neq j}\left[\phi_i^*(k, r_i, \theta_{\boldsymbol{r}_i}^{\boldsymbol{k}}) \cdot \phi_j(k, r_j, \theta_{\boldsymbol{r}_j}^{\boldsymbol{k}})\right]$$

where *Re* is the real part of complex expression.

The first term in this equation corresponds to the photoemission intensity distribution in absence of any scattering by neighbouring atoms. The information about spatial distribution of atoms relative to the emitter is in the second term. The third term describes the diffraction of waves scattered by ith atoms at jth atoms and, hence, it contains information about the spatial distribution of the atoms relative to one another.

Two major approaches used in XPD analysis follow from Eqn (5); they are based on measurement of the intensity $I(\boldsymbol{k})$ as a function of either the magnitude or the direction of wave vector. In the former case, the dependence of the exponential term $\exp\{\text{i}[kr_i(1 - \cos\theta_{\boldsymbol{r}_i}^{\boldsymbol{k}})]\}$ on the scalar quantity $k = |\boldsymbol{k}|$ is used in the structural analysis. For this purpose, a tunable X-ray source is employed in experiments, and the intensity is recorded as a function of kinetic energy of photoelectrons at a fixed observation angle.[25,26] Such experiments are often called energy-scanned photoelectron diffraction. The experiments of this type can only be carried out at synchrotron radiation centres where it is possible to vary X-ray radiation energy from tens of electron volts to a few keV. This option of photoelectron diffraction is not considered in this review.

The second approach to gaining structural information is varying the direction of the wave vector with the magnitude remaining unchanged. The vector direction relative to the atomic ensemble is described by the dependence of the exponential term $\exp\{\text{i}[kr_i(1 - \cos\theta_{\boldsymbol{r}_i}^{\boldsymbol{k}})]\}$ on the $\theta_{\boldsymbol{r}_i}^{\boldsymbol{k}}$ angle. As the wave vector direction coincides with the radius-vector going from the emitter to the detector, the angle $\theta_{\boldsymbol{r}_i}^{\boldsymbol{k}}$ can be changed by rotation of the sample relative to the detector. The experiments of this type are called angle-scanned XPD. If a two-dimensional electron detector is used, it is sufficient to rotate the sample around the normal to its surface. In this case, both synchrotrons and laboratory sources of X-ray radiation are suitable. Different types of the experimental setup for angle-scanned XPD are considered below.

Analysis of Eqn (5) indicates that a separated phase component of the XPD pattern can be considered as a hologram.

Thus, as follows from Eqn (5), the photoemission intensity distribution reflects the spatial structure of the local environment of the chosen emitter atom. If there is a definite pattern in the arrangement of the surface cluster atoms relative to the chosen emitter, their contributions form the oscillating component of the intensity dependence on the wave vector. The intensity measured in the XPD experiment is a superposition of intensities $I(\boldsymbol{k})$ produced by separate emitting atoms, each having its own local environment. Therefore, the diffraction effects related to scattering by the local environment are most pronounced for the systems with an ordered arrangement of emitting and scattering atoms. As a result, the main objects of studies with the use of XPD are surfaces of single crystals, ultrafine epitaxial layers, films adsorbed on single crystals, *etc*. For these systems, the normalized anisotropy of spatial emission of photoelectrons

$$\frac{I_{\max} - I_{\min}}{I_{\max}} = \frac{\Delta I}{I_{\max}} \times 100$$

exceeds ~50%–70%. The examples of experimentally obtained and calculated 2π-projections of photoemission $I(\boldsymbol{k})$ for a perfect single-crystalline surface of Cu(111) are shown in Fig. 3.

It is of interest to compare X-ray photoelectron diffraction with other related techniques of structural analysis such as LEED and EXAFS (extended X-Ray absorption fine structure) (Fig. 4). Note that EXAFS is a method for structural studies in the bulk, it enables one to investigate the structure of the local environment of the chosen type of atoms and is used in the studies of single crystals, polycrystalline and amorphous samples, solutions an so on. The major advantage of EXAFS is its versatility. Its main disadvantages consist in necessity of the use of synchrotron radiation and complexity in processing and interpretation of experimental data. A monochromatic beam of low-energy electrons (30–200 eV) is used in the LEED experi-

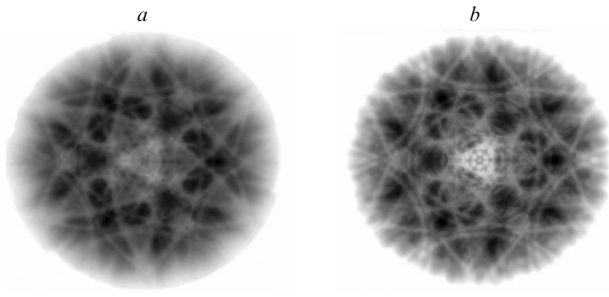


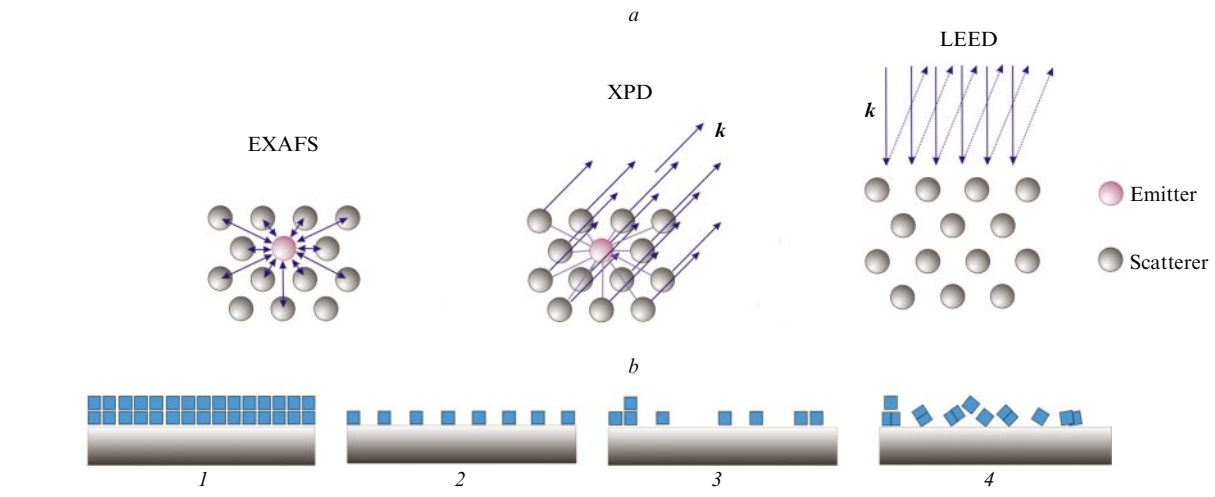
Figure 3. Experimental (*a*) and calculated (*b*) stereographic projections of Cu3p photoelectron diffraction pattern for the Cu(111) surface.[27]
(*a*) The projection was obtained using a toroidal analyzer (BESSY II, Berlin) at the exciting synchrotron radiation energy of 600 eV; (*b*) the calculations were carried out using the EDAC (electron diffraction in atomic clusters) programme in the multiple electron-scattering approximation.

ments, it impinges on the surface and after scattering acquires the information about it. This technique provides the information concerning the long-range order of the surface structure, but it does not give chemical information, *i.e.*, it does not distinguish particular positions of atoms of different types. The obvious advantages of LEED are the possibility to get structural information using this technique in the online mode and good mathematical basis for the interpretation of diffraction images.

Thus, in comparison with LEED, XPD has, on the one hand, a significant disadvantage consisting in long duration of the experiment, but on the other hand, a distinct advantage, namely, the possibility to analyze structural positions of atoms of a given type and, moreover, to discern between positions of atoms of the given type in different chemical states. In other words, XPD is one of the rare techniques providing chemical information about surfaces in addition to structural information.

Due to the sensitivity of XPD to the geometry of the local environment, it is possible to analyze structures of both perfect single crystal faces and other objects such as surface clusters with structure of the same type (not necessarily periodic) and orientation (see Fig. 4), whose size can be very small (less than 10 Å). These cluster are formed at early stages of growth of epitaxial films.[28–30] Another suitable object is adsorbed molecular layers, where the adsorbed molecules do not form an ordered surface superstructure, but are situated at certain positions relative to the atoms of the first substrate layer.[9, 21, 22] The structural analysis of such small atomic surface objects is possible with XPD only.

Structural analysis of polycrystalline and amorphous surface layers cannot be performed using XPD since spatial geometry of the local environment (in the coordinate system 'sample surface – photoemission wave ***k***') varies in a random way depending on the emitting atom position and the set of



EXAFS	Yes	Yes	Yes	Yes
XPD	Yes	Yes	Yes	No
LEED	Yes	Yes	No	No

Figure 4. Illustration of capabilities of EXAFS, XPD and LEED in the study of surface structure of solids (http://www.sussex.ac.uk/Users/qc25/teaching/Surfsci2.pdf).
(*a*) The basics of the methods: EXAFS is based on the analysis of oscillations of X-ray absorption coefficient near the absorption edge due to interference between the diverging wave of the emitted electron and a part of the same wave scattered by neighbouring atoms in backward direction; XPD is characterized by clear spatial anisotropy of the photoelectron emission from the surface due to scattering and interference of the electron wave outgoing from the emitting atom at the atoms of the local environment; LEED is the diffraction of low-energy electrons elastically scattered by the surface layers.
(*b*) The possible structures of surfaces: (*1*) a single-crystal surface or epitaxial layers, (*2*) periodic structures with ordered arrangement of atoms and atomic clusters, (*3*) non-periodic structures with the same structure and orientation of atomic clusters, (*4*) surface structures without ordering or mutual orientation. 'Yes' and 'No' express the applicability of the particular method to the study of the particular surface.

all possible orientations of scattering clusters with the same (or similar) structure does not give an oscillating component, which depends on the phase factor $\exp\{i[kr_i(1-\cos\theta^{\boldsymbol{k}}_{\boldsymbol{r}_i})]\}$. Clearly, only objects which possess a sufficient number of emitting atoms with similar spatial geometry of the local environment or have a limited number of structurally non-equivalent positions of emitting atoms are amenable for determination of structural parameters of surface clusters with the use of XPD.[20]

2. Experimental implementation

Various schemes are used to obtain the experimental diffraction pattern by means of angle-scanned XPD. The simplest scheme can be implemented using a laboratory spectrometer with hemispherical electrostatic electron analyzer (Fig. 5*a*). In this scheme, the position of the X-ray source and electron analyzer relative to the sample is fixed; to obtain the complete 2π diffraction projection, it is required to rotate the sample over the azimuthal (φ) and polar (θ) angles and reduce the solid angle of photoelectron collection (Ω). It was shown that the decrease in the Ω angle can be achieved by disabling the focusing lenses of the analyzer,[31, 32] in this case the collection angle is defined by the distance from the sample to the analyzer ($\sim$600 mm) and the size of entrance aperture of the analyzer (3 mm); as a result, the electron collection angle can be decreased from $\sim$25 to $\sim1^\circ$. This scheme is simple and makes it possible to switch from the XPS mode with angle averaging to XPD with high angle resolution. In the latest generation of electron spectrometers, the photoelectron collection angle is controlled by a set of focusing lenses.

An XPD experiment is carried out in the following way. Scanning over the azimuthal angle φ from 0 to 360° (if the crystal symmetry is known, the scanning range can be reduced) in certain $\Delta\varphi$ increments, *e.g.,* of 1°, is performed at a fixed polar angle θ. Then the polar angle is changed (also by 1°), and scanning over the azimuthal angle is repeated, the typical range of variation of the polar angle is usually 0–80° relative to the normal to the sample surface. In the case of XPD with resolution of chemical (or magnetic) states, the rotation of the sample is accompanied by recording of the X-ray photoelectron spectrum for the element of interest in each point (θ, φ). The measurements afford an array of ten (or more) thousands of spectra. Each spectrum is decomposed into components responsible for nonequivalent forms of the element, the intensity of each band is measured, and the arrays of intensities of separate chemical states $I(\theta, \varphi)$ are formed. Then, the diffraction 2π projections of non-equivalent states of the chosen elements are constructed.

At present, there are electron spectrometers specially designed for the analysis of angle dependences of X-ray photoelectron spectra. An example of such spectrometer is Theta Probe (USA) (Fig. 5*b*), which is able to record an array of electron spectra in a 60° polar angle range in $<1^\circ$ increments owing to a modified system of lenses. To obtain the complete diffraction pattern, it is sufficient only to scan 360° of the azimuth angle. However, the central part of the XPD pattern from 0 to 20° is missing.

Toroidal electron analyzers (Fig. 5*c*) providing two-dimensional distribution of photoemission are of great interest for XPD. Such analyzers operate, for instance, in one of the lines of the BESSY II synchrotron storage ring (Germany),[27, 33] and in the BL25SU line of Japanize synchrotron SPring-8.[34, 35] A specific feature of instruments of this type is the possibility to record full 2π patterns of electron photoemission for polar and azimuthal angles in the 0–90° and 0–360° ranges, respectively. An example of experimental scan of diffraction pattern of Bi4f photoelec-

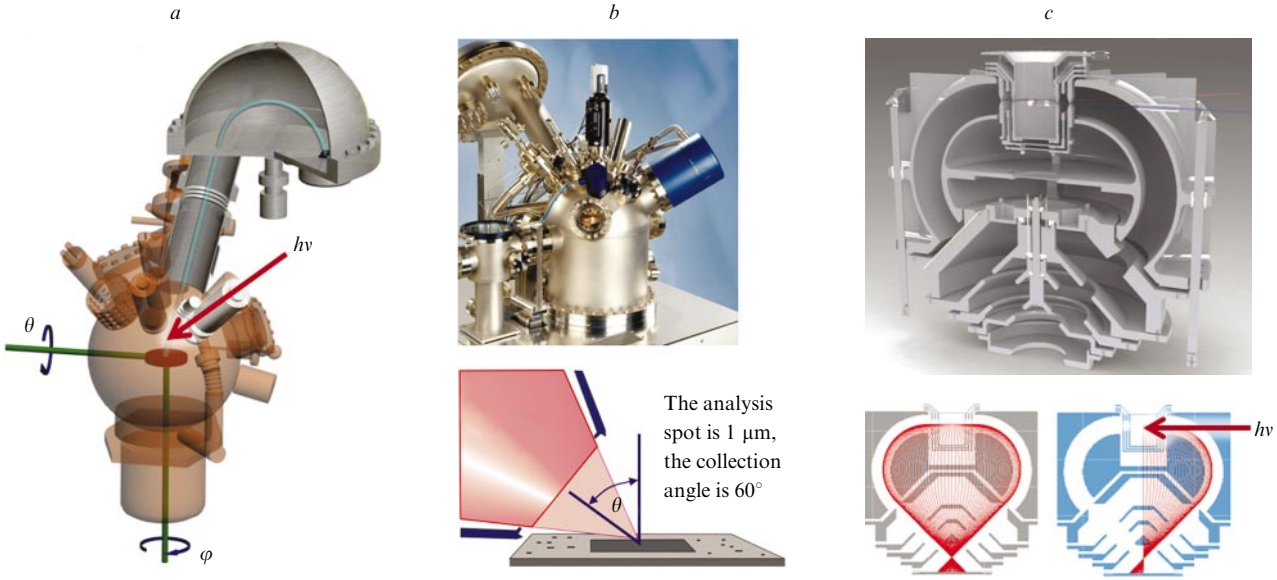


Figure 5. Types of spectrometers used in recording of XPD patterns by angle scanning.
(*a*) VG Escalab MK II laboratory electron spectrometer;[31, 32] (*b*) Theta Probe specialized electron spectrometer for studies of angle dependences in XPS; (*c*) basic design of toroidal electron spectrometer for ARPES and XPD studies; in the bottom part, two sections of toroidal analyzer are given and trajectories of photoelectrons emitted by the sample surface under the influence of photons (synchrotron beam is marked by the arrow) are shown, the photoelectrons are detected at the analyzer outlet using a multichannel plate.[27]

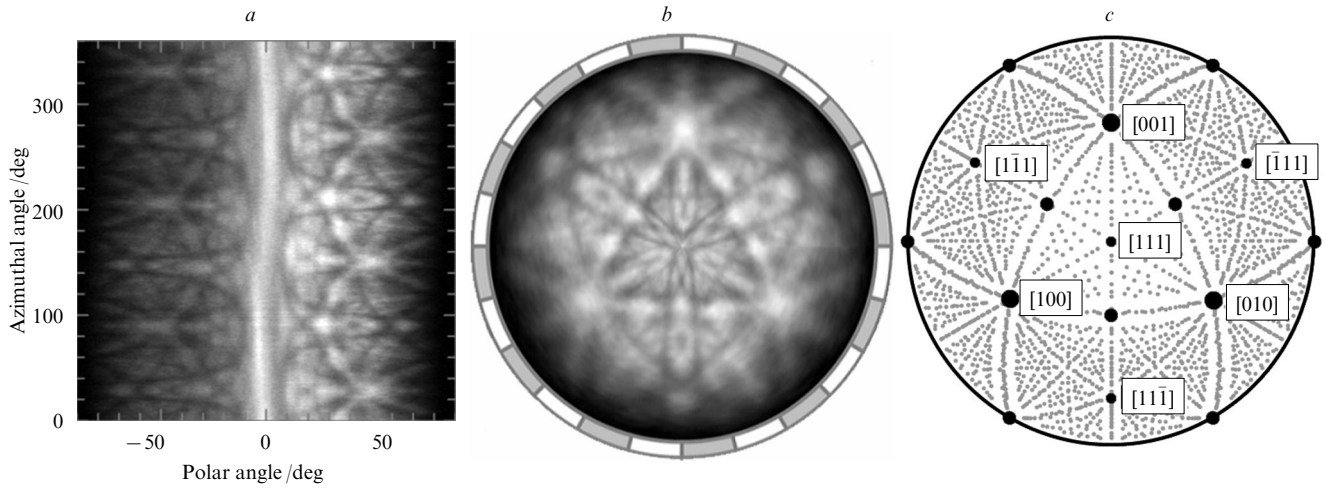


Figure 6. Experimental scan of the Bi4f photoelectron (E = 742 eV) diffraction pattern for the Bi_2Te_3(111) surface obtained with the use of a toroidal analyzer at the synchrotron centre BESSY II (*a*), stereographic projection constructed from this scan (*b*) and model stereographic projection of the Bi_2Te_3(111) plane (*c*).†

trons obtained with the use of a toroidal analyzer for a Bi_2Te_3(111) surface is shown in Fig. 6.

Note that the duration of scanning with 1° angle resolution using toroidal analyzer is ~1 h; during this period, the sample makes a full rotation around the normal to the surface by the azimuthal angle. Thus, the duration of the experiment is comparable with recording of the conventional XPS spectrum. In the course of subsequent processing, the experimental scan is transformed to more easily understandable stereographic projection. In our opinion, these instruments are currently most convenient and accurate in getting XPD patterns.

3. Structural analysis

The information about the structure of the surface layers under study is extracted from experimental data obtained by X-ray photoelectron diffraction. The methods for structural XPD analysis are well developed and described (see, for instance, Refs. 17, 19 and 21). Depending on the depth of treatment, precision and versatility, one can distinguish three qualitative levels of analysis of the experimental XPD data. The first (simplest) level is based on determination of the symmetry of the diffraction pattern and angles of the main scattering peaks. This approach gives quite adequate ideas about the surface structure in some cases. At the next level, quantitative theoretical calculations of XPD pattern are conducted for model clusters describing the surface. The used theoretical models contain a series of approximations, which affect the accuracy of the final result and the calculation speed. The structural parameters are refined based on the *R*-factor, which is a measure of agreement between the theoretical and experimental XPD data. The third level is based on the solution of the direct problem of restoration of the structure of the scattering cluster surrounding the emitting atom from the XPD data with the use of formalism of photoelectron holography. This level is not more precise than the theoretical calculations; however, it makes the first step towards determination of the scattering cluster geometry and allows estimating the interatomic distances. Actually, both approaches, the model calculations and holography, are required to determine the surface structure parameters, especially, in complicated cases, where relaxation effects and structural transformations on the surface take place.

Consider the main features of X-ray photoelectron diffraction and the possibilities and constrains of XPD structural analysis of surfaces defined by these features.[20] An important specific feature of XPD consists in the dependence of the complex factor of atomic scattering $f_i(\theta^{\boldsymbol{k}}_{\boldsymbol{r}_i})$ [see Eqn (4)] on the photoelectron kinetic energy (E) and the scattering angle ($\theta^{\boldsymbol{k}}_{\boldsymbol{r}_i}$).

The first calculations of atomic scattering amplitudes $|f_i(\theta^{\boldsymbol{k}}_{\boldsymbol{r}_i})|$ were performed in the 1980s[36, 37] to show that the angle dependence of $|f_i(\theta^{\boldsymbol{k}}_{\boldsymbol{r}_i})|$ is substantially anisotropic if photoelectron kinetic energies are $\geqslant$1000 eV (Fig. 7). The non-zero values of atomic scattering amplitudes correspond to narrow range of the $\theta^{\boldsymbol{k}}_{\boldsymbol{r}_i}$ angles close to the direction to the scattering atom; the effects of reverse scattering are practically absent. Thus, the effects from interference of waves scattered by the local environment of the emitting atom are negligibly small at these energies, and photoemission intensity maxima are only observed in the directions of forward scattering ($\theta^{\boldsymbol{k}}_{\boldsymbol{r}_i} \approx 0°$), which correspond to the directions $\boldsymbol{r}_i$ to the atoms surrounding the emitter. Additionally, the scattering phase shift becomes insignificant at small scattering angles in the forward direction.[38]

This effect was called the forward-scattering approximation. In some cases, this approximation can be used in the structural analysis since the distribution patterns of major photoelectron intensity maxima almost entirely reflect the geometry of the local environment of the emitter. The forward-scattering approximation is most often used to determine the symmetry and bond parameters of adsorbed molecular systems.

† The data were obtained by the authors in collaboration with Doctor of Chemical Sciences L V Yashina (Department of Chemistry, Lomonosov Moscow State University).

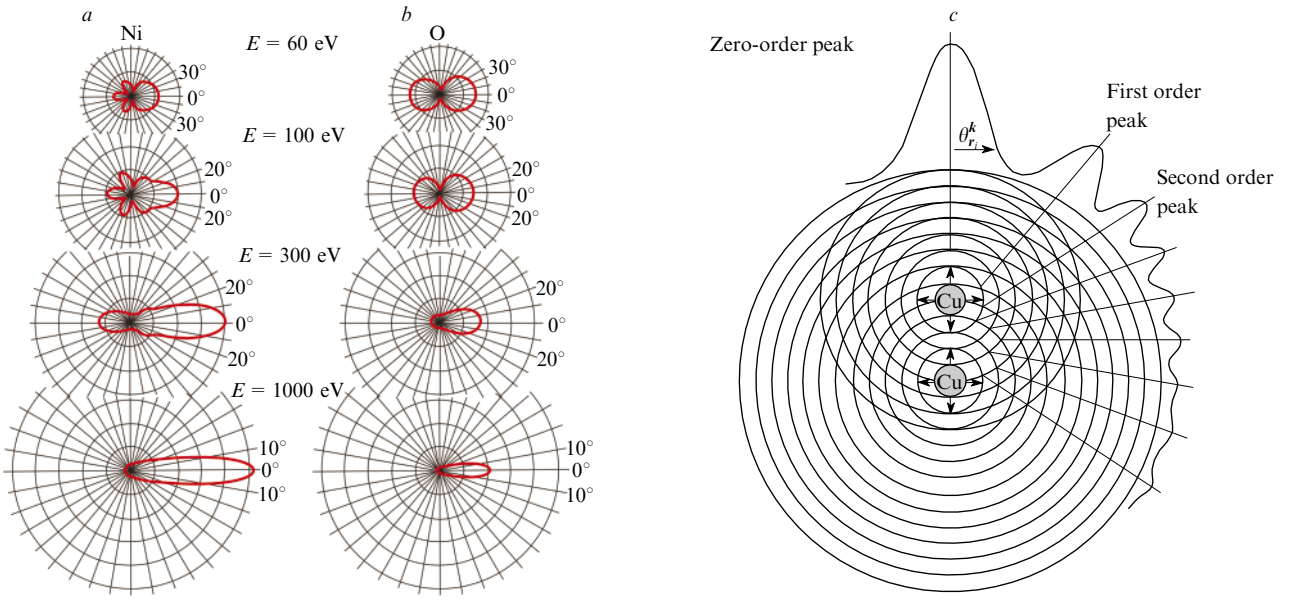


Figure 7. Angular distribution of the amplitude $|f(\theta^{\mathbf{k}}_{r_i})|$ of the electron scattering by nickel (*a*) and oxygen (*b*) atoms at $E = 60-1000$ eV and scheme of interference of two ideal spherical waves outgoing from the emitting copper atom and a scattering copper atom with a zero scattering phase shift (*c*).[37, 38]
The angle $\theta^{\mathbf{k}}_{r_i} = 0^\circ$ corresponds to the direction of forward scattering, if kinetic energy of emitted electrons is high, the zero-order peak is strongest. The peaks of the first and higher orders become more intense at low photoelectron energies.

This approximation is also used in the analysis on interatomic distances in surface layers of single crystals and in epitaxial films. The XPD patterns for single crystal surfaces fully correspond to stereographic projections (see Fig. 6 *c*).[17, 39, 40] In some uncomplicated instances, it is possible to determine the type of structure and crystallographic orientation and to estimate the lattice parameters directly from the experimental XPD pattern. The use of forward-scattering approximation and stereographic projections proved to be fruitful for studies of phase transformations at single crystal surfaces, especially, if they are characterized by rigorous orientational interphase relationships, and for analysis of structural regularities of epitaxial nanolayer growth. In the case of ordered adsorbed systems, location of the adsorbate atoms on the single crystal surface can be qualitatively characterized in the framework of this approximation.

At the same time, as it was noted by Westphal,[19] this version of photoelectron diffraction is based on the zero-order interference (see Fig. 7 *c*), which does not depend on the electron wavelength. Therefore, this version is not genuine diffraction as the peaks of higher orders are not considered.

Since the forward-scattering approximation is applicable only to high-energy electrons, this approach was further developed in laboratories equipped with spectrometers having one or two constant-energy photon sources such as MgK_α (1253.6 eV) and AlK_α (1456.6 eV). At such high energies of exciting photons, the kinetic energy of electrons emitted from core levels is 300 eV or more, therefore the advantages of this approach can be used.

The classic study of Saiki *et al.*[41] represents an example of application of the forward-scattering approximation to analysis of molecular bond orientation on surfaces. The authors studied CO adsorption on the Fe(001) surface using XPD. For the CO/Fe(001) adsorption system, it is known that CO molecules are bound to the metal surface through carbon atoms. Since oxygen atoms are located above carbon atoms, photoemission of oxygen atoms exhibited no effect of forward scattering. On the contrary, electrons emitted by carbon atoms were scattered and produced signals in the direction of the C–O bonds. Figure 8 *a*,*b* shows the C1s/O1s signal dependences on polar angles for two azimuthal directions, [1$\bar{1}$0] and [100], and the dependence of the C1s emission intensity for polar angle $\theta = 35^\circ$. As can be seen, a strong anisotropy of the C1s/O1s emission intensity ratio is observed in the [100] azimuth direction with maximum at $\theta = 35^\circ$ relative to the surface. At the polar angle $\theta = 35^\circ$, there are two strong maxima in the dependence of the C1s intensity on the azimuthal angle, they correspond to the [100] and [010] azimuths. Analysis of obtained dependences definitely indicates closer location of carbon atoms to the single crystal surface and orientation of CO molecules in the (010) plane at a $35 \pm 2^\circ$ angle relative to the Fe(001) plane. The arrangement of CO molecules on the Fe(001) surface is shown in Fig. 8 *c*.

The forward-scattering approximation approach was popular at early stages of development of the XPD technique and was successfully applied to study the NO/Ni(100) system[42] and to analyze the geometry of more complex molecules such as the formate on the (110) surface of titanium dioxide.[43]

A necessary condition for the application of the forward-scattering approximation is as follows: the emitting atom must be located below the atom that scatters the electron wave. In the case of systems with adsorbed layers where separate atoms but not molecules are adsorbed on the surface, atoms of the crystal outer layer can act as emitters. It is possible if the states of atoms of the outer layer differ from the states of other atoms of the crystal and

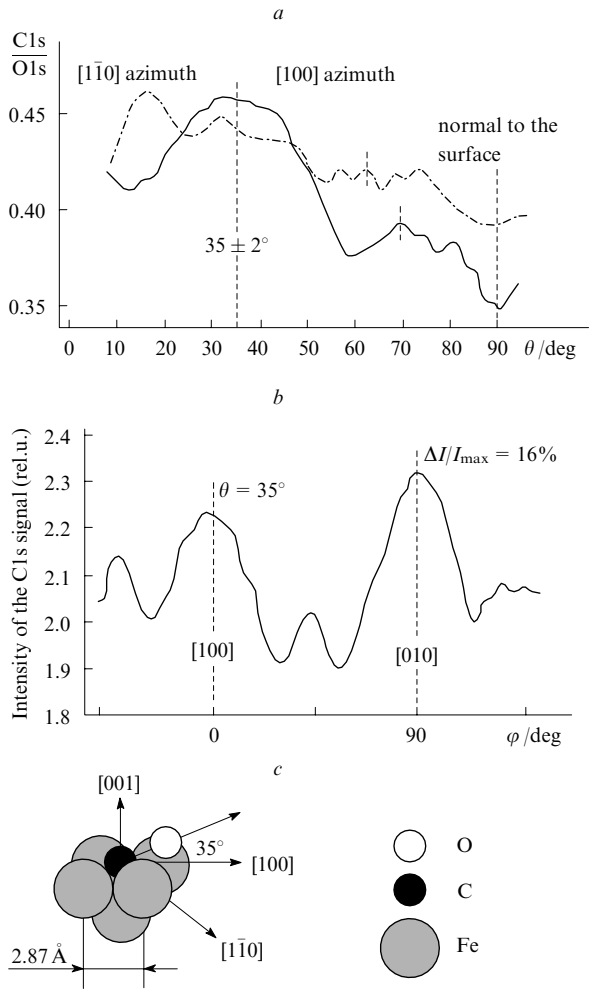


Figure 8. Results of XPD study of CO adsorption on the Fe(001) surface.[41]
(*a*) Relative intensities of the C1s/O1s signals *vs*. polar angles; (*b*) intensities of the C1s signal *vs*. azimuthal angles; (*c*) model CO adsorption on the Fe(001) surface.

their spectrum can be distinguished against the intensive spectrum of the crystal matrix.

A characteristic example of the use of this approach is given in the study of Daimon *et al*.[44] in which the arrangement of the adsorbed (1 × 1)O/W(110) layer was ascertained using XPD with resolution of W4f states in the tungsten spectrum (Fig. 9). The authors succeeded in obtaining the 2π projection for W4f photoelectrons of only the upper layer of the tungsten atoms that are chemically bonded to oxygen atoms. Using the forward-scattering approximation, they analyzed the experimentally obtained 2π projection of W4f photoelectron diffraction on the tungsten surface and determined structural parameters of the location sies of ordered oxygen atoms.

A similar approach was used in a study of CO and N_2 chemisorption on the Ti(0001) surface.[32,33] In this system, carbon, oxygen and nitrogen atoms, after dissociation of the molecules on the surface, are partially incorporated into the octahedral interstitial sites of the titanium lattice below the crystal surface. The XPD analysis with resolution of the C1s, N1s and O1s chemical states made it possible to determine the adsorbate location sites both on and below the surface. Of recent studies, it is worthwhile to note the study[45] of the adsorbed O/Nb(110) layers. The niobium atoms of the first layer of the Nb(110) surface responsible for intrinsic energy states in the Nb3d spectra were used as emitters.

Besides the systems with adsorbed layers, single crystal surfaces, epitaxial films and subsurface structures can be studied in the framework of forward-scattering approximation. Recall that, according to the approximation, the angular positions of the scattering intensity maxima reflect the geometry of the short-range order for the given emitting atom and coincide with the directions of the close packing and the planes in the crystal which pass through the sites of this atom. If emitting atoms with non-equivalent short-range geometry exist for the same chemical state, the total

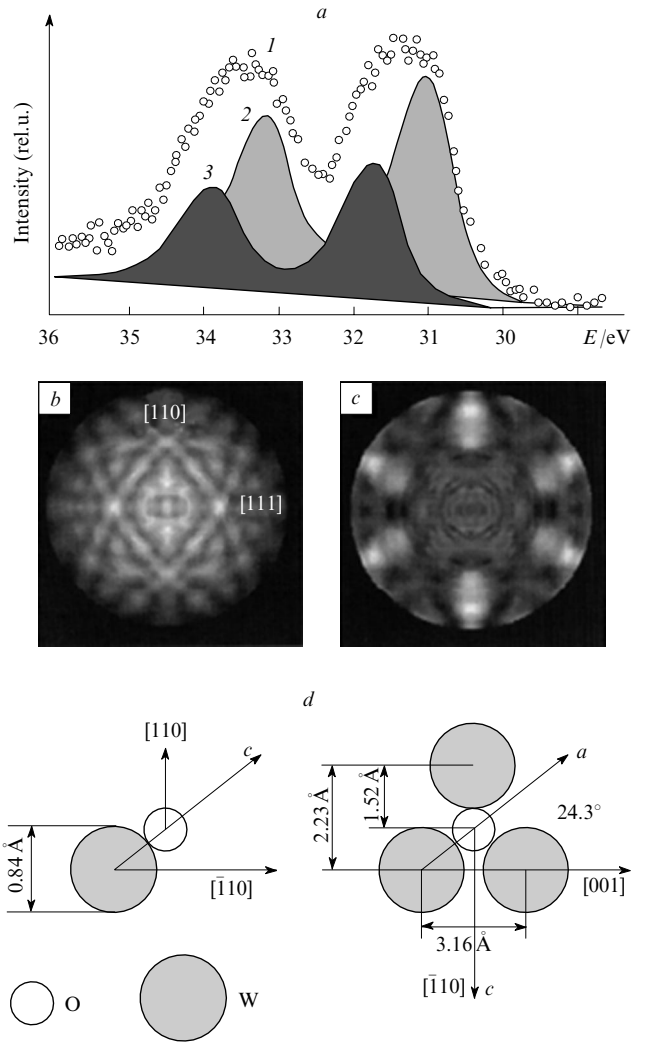


Figure 9. Results of XPD study of the (1 × 1)O/W(110) system.[44]
(*a*) Experimental X-ray photoelectron spectrum of tungsten (*1*) with distinguished W4f states of the first surface monoatomic tungsten layer chemically bonded to oxygen atoms (*2*) and single crystal bulk (*3*). Diffraction patterns of W4f photoelectrons: (*b*) bulk component; (*c*) component from the first tungsten monolayer bonded to oxygen; (*d*) location of oxygen atoms on the W(110) surface.

XPD pattern (which is a superposition of scattering intensities for all the emitters) reflects the whole set of the close packing directions for the atoms of this type. By comparing the 2π projections of photoelectron intensity distributions with stereographic projections, one can determine crystallographic orientations of single crystal surfaces. This problem can be solved most easily for single-component structures or the structures in which the short-range geometry of all the emitters is the same for any chemical state of these emitters. In this case, the only XPD pattern is required even for a multicomponent system. The application of this approach was demonstrated in a series of studies of single crystals of $CuInSe_2(112)$,[39] $Fe/Cu_3Au(001)$,[46] Ru(0001) and Ni(001),[12] Ni(110) [16] and Nb(110).[40]

It is impossible to determine the structural type of single crystal surface unambiguously in the forward-scattering approximation because it neglects the scattering effects related to different types of atoms in structurally equivalent sites (*i.e.* to ordering), to small deviations of lattice parameters, *etc*. Nevertheless, analysis of the experimentally obtained XPD patterns in the framework of this approximation affords information about the short-range order geometry and the structure of the surface layer in the case of not sophisticated structures of known composition and, therefore, it can be useful for identification of such structures.

Consider the surface of a FCC crystal as an example.[19, 47] The emitting atom is located in the second surface layer of three (in the general case) layers. The geometry of the atom environment is illustrated by Fig. 10. For example, electrons emitted by an atom in the Ni(111) crystal are scattered by the neighbouring atoms.[47] At high kinetic energies, the maximum scattering occurs in the directions from the emitter to the surrounding atoms. The positions of these atoms can be defined through interplanar spacings and θ and φ angles (Table 1).

The directions to the atoms of the fourth local environment coincide with the directions to the atoms of the first one. The experiment and calculations of photoelectron diffraction for the emission from the $Ni2p_{3/2}$ levels of the Ni(111) surface are understandable from the scheme shown in Fig. 10. As can be seen, determination of the azimuthal and polar angles of the major reflections in the experimental XPD pattern is sufficient to confirm or refute the simple picture of the forward scattering for the zero-order diffraction (at high kinetic energy of photoelectrons) on the Ni(111) surface.

At present, the primary analysis of diffraction patterns in the forward-scattering approximation can be carried out by computer programmes used to construct stereographic projections for model clusters that describe the surface without diffraction effects. An example of such a projection for Ni(111) is shown in Fig. 10 *b*. The convenience of this approach consists in the possibility to mark (with colour or size) the reflections corresponding to certain scattering atoms from the emitter environments of different orders. In the case of multicomponent crystals or complex adsorbed systems, this approach to the primary analysis of XPD patterns seems helpful.

Table 1. The θ and φ angles determining the positions of atoms.[47]

Local environment	θ /deg	φ /deg
First	35.5	0, 120, −120
Second	54.7	60, 180, −60
Third	20	60, 180, −60
Fourth	35.5	0, 120, −120

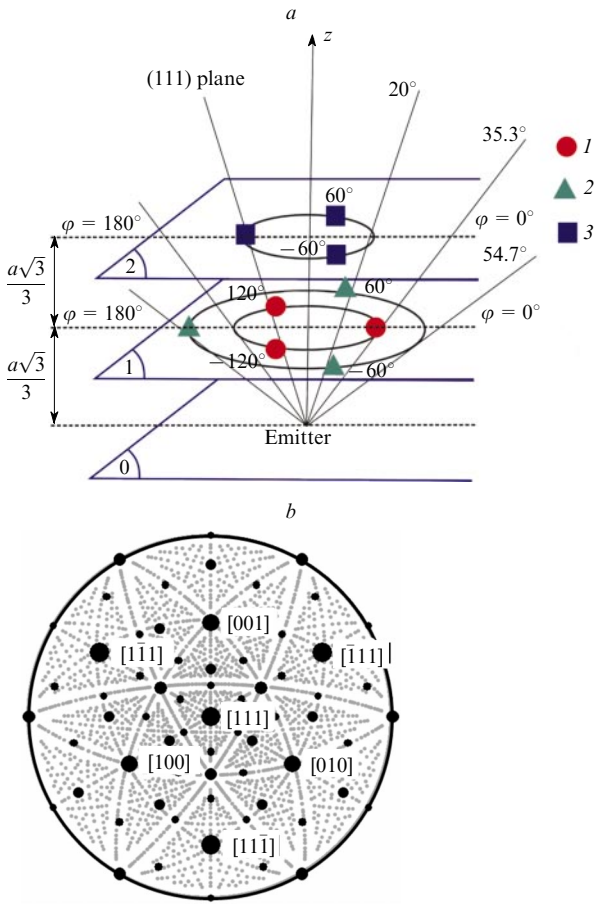


Figure 10. Schematic view of three layers of the (111) surface of an FCC crystal.
(*a*) The emitting atom is located in the second layer below the surface; atoms of the first (*1*) and second (*2*) environments are in the layers above the emitting atom, atoms of the third (*3*) environment are above the surface;[47] (*b*) stereographic projection calculated for model Ni(111) cluster.

Return to Eqns (4) and (5). The effect of forward scattering, which occurs only at $E \geqslant 1000$ eV, has been discussed above. In the range of high kinetic energies of photoelectrons, a rough approximation of photoemission from s level is also valid.[39, 48–50] The type of final states of the emitted electron (l_f) and their interactions are not taken into account in this approximation; therefore, the dipole matrix element can be omitted. As a result, interference effects for waves scattered at the local environment become negligible in this region of energies.

Studies of Fadley and co-workers [17, 51] can be considered as a limiting case of the use of high energy photoelectrons. Hard X-ray synchrotron radiation with photon energy ($E_{h\nu}$) of 5–20 keV or radiation of laboratory sources such as $CrK_{\alpha 1,2}$ ($E_{h\nu}$ = 5.417 keV) was employed to excite the photoemission. This resulted in a 2–3-fold increase in the analysis depth (up to 10 nm and more), which is very

important, for example, in studies of thin-film structures. At such high energies of emitted photoelectrons, the effects of forward scattering by the nearest atoms not merely predominate but completely determine the structure of XPD patterns. This technique was called hard X-ray photoelectron diffraction (HXPD). Owing to the increase in the mean free path in HXPD, the number of emitting atomic layers increases, and the Bragg scattering by the crystal planes starts to have effect. Taking this into account, the photoelectron diffraction is best regarded as a process of multiple Bragg scattering resulting in the appearance of Kikuchi bands. The analysis of results of theoretical modelling for HXPD showed that this technique can be very sensitive to the type of the element and the positions of atoms in the lattice (such as substitutional or interstitial sites), as well as to the lattice relaxation.[17]

As the photoelectron kinetic energy decreases below 1000 eV, the role of interference effects (see Fig. 7) and angular momenta of initial and final states of the emitted photoelectrons in both the forward and backward scattering increases. In this case, complete quantitative calculations of photoemission intensity $I(\boldsymbol{k})$ are required to analyze experimental XPD patterns.

To demonstrate the XPD pattern changes depending on the photoelectron kinetic energy, we will consider our own results of the $Bi_2Te_3(111)$ surface studies. The experimentally obtained and simulated XPD patterns for Bi4f electrons with kinetic energy increasing from 202 to 742 eV are shown in Fig. 11. The Bi4f binding energy (E_b) is $\sim$160 eV. The energy of photons of exciting synchrotron radiation was varied to change the kinetic energy of electrons. It can be seen that at high kinetic energies of photoelectrons, the XPD pattern is clear-cut, and the reflections corresponding to the major directions of close packing of atoms in the Bi_2Te_3 lattice are distinguished. At low energies ($\leqslant$ 500 eV), the patterns becomes more sophisticated due to intensification of effects of the first, second and higher orders, as well as effects of backward scattering. Analysis of such patterns from the position of the forward scattering is impossible, and carrying out of model calculations is needed.

The interest in XPD at medium and low kinetic energies of electrons is very high. Intensification of backward scattering effects is required, for example, in gas adsorption studies, where the adsorbate atoms are used as sources of photoemission, and the diffraction pattern from scattering by the substrate atoms is analyzed. Weakening of the maximum of forward scattering and intensification of the interference effects of the first, second and higher orders (see Fig. 7 *c*) form the basis of implementation of photoelectron holography. From the experimental point of view, the interest in XPD at low electron kinetic energies is caused, *inter alia*, by high intensity of synchrotron radiation at low E_{hv} values, which has a positive effect on the precision of XPD data.

4. Numerical simulation of photoelectron diffraction

Quantitative calculations of XPD are needed in order to understand the nature of photoelectron diffraction maxima and compare the experimentally obtained results with theoretical predictions for the model surface structure. At the initial stage of development of XPD calculations, the model of single scattering plane wave [single scattering cluster–spherical wave (SSC–SW)] was employed [see Eqns (1)–(5)]. This approach was used until the mid-1980s, mainly, for investigation of the adsorbed gas/metal systems and also various single-crystal surfaces.[15, 52, 53] The qualitative correspondence between the experiment and the theory was quite good; however, the anisotropy of photoemission intensity in the forward direction was overestimated and divergence in the fine structure of the peaks was observed. A substantial difference between the results of calculations in the scattering plane wave approximation and

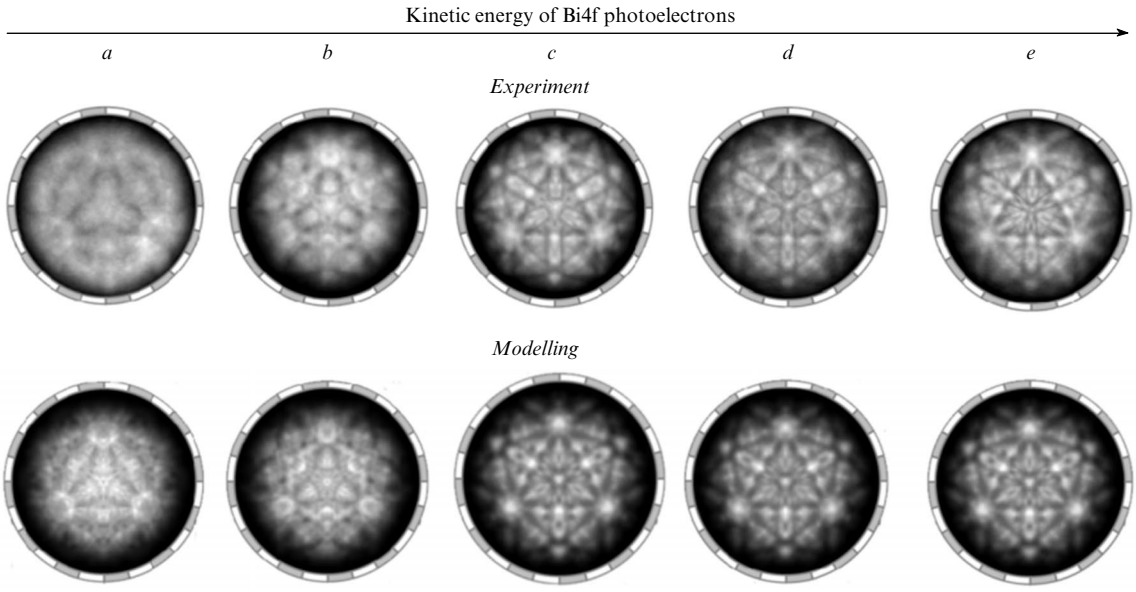


Figure 11. Bi4f photoelectron diffraction patterns obtained experimentally and calculated in the multiple scattering approximation for the $Bi_2Te_3(111)$ surface at E = 202 (*a*), 302 (*b*), 542 (*c*), 642 (*d*) and 742 eV (*e*).
The experiment was carried out with the use of the toroidal analyzer (BESSY II), the calculations were performed using the EDAC code.

experimental data was revealed for the (2×2)S/Ni(001) system, indicating the restricted applicability of this approach to the quantitative structural analysis of surfaces.

The capabilities and limitations of the SSC–SW approximation in the XPD studies were considered in detail in a review.[15] Particularly, it was noted that in the region of moderate kinetic energy (< 300 eV), the assumption of photoemission from the s level proved to be unsatisfactory; its limitations in interpretation of the data of photoelectron and Auger electron diffraction were demonstrated in many experimental and theoretical studies.[39, 46, 50, 54, 55] Particularly, substantial discrepancy was found between forward scattering intensities measured in experiments with single crystals at low kinetic energies of Auger electrons (65 eV) and calculated in the framework of the scattering plane wave approximation: only minima of scattering intensity were observed instead of expected maxima.[54, 55] The analysis of the whole set of the data showed that this was due not only to low kinetic energy but also to the character of the wave source, *i.e.*, the initial and final angular momenta of the emitted electron.[39, 50] Calculation in the single scattering spherical wave approximation confirmed that the type of the final state of the emitted electron with $E < 100$ eV (the wave type is s, p, d, f, g or h) determines the observed diffraction pattern (Fig. 12). Accurate description of the initial and final states of photoelectron wave can also be necessary if kinetic energies are high, especially, in the case of precision structural XPD studies.[49, 56]

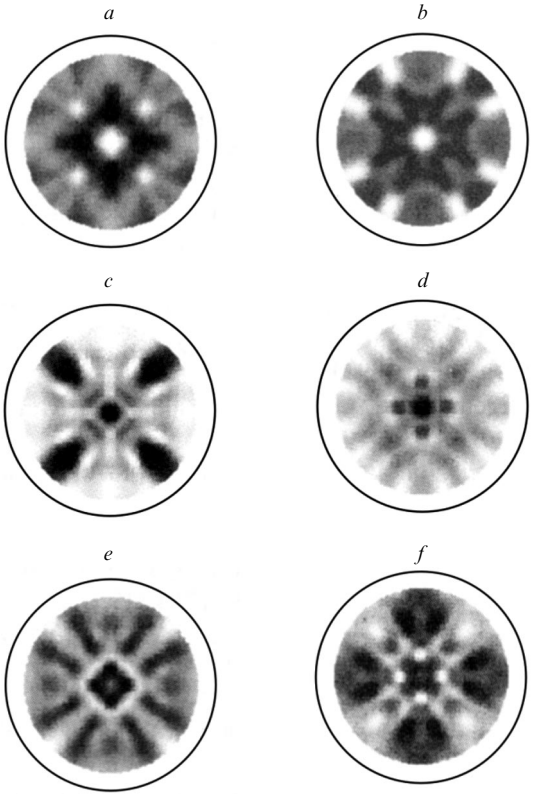


Figure 12. Calculated 2π projections of electron diffraction ($E = 60$ eV) for the Cu(001) surface in the single scattering spherical wave approximation.[39]
The type of electron wave is s (*a*), p (*b*), d (*c*), f (*d*), g (*e*), h (*f*).

Thus, XPD modelling in the scattering plane wave approximation gives no good result in quantitative structural analysis, especially, in the case of low kinetic energies of photoelectrons. At present, realistic quantum mechanical models have been developed that describe photoelectron scattering by spherical waves in the approximation of single and multiple scattering, and based on these modes, so-called scattering spherical wave methods have been developed.[57–60] The matrix formulation of separable Green's functions[48, 49, 60] and Taylor-series magnetic quantum number expansion (TS-MQNE)[57, 59] are approximate schemes which are most widely used for XPD simulation. Both schemes approximate the scattering system by a cluster consisting of separate atoms; this corresponds to the local type of formation of diffraction effects in the surface layers. One of advantages of the cluster approaches consists in the capability of modelling separate structural defects (of both topological and compositional types). At the same time, like all quantum chemical approaches, these methods do not take into account the statistical character of structural defect distribution. The key provisions for the application of separable Green's functions to simulation of photoelectron diffraction in the single scattering spherical wave approximation are considered by Kaduwela *et al.*[48]

Numerical simulation of XPD in scattering spherical wave approximation (even in the single scattering approximation) significantly enhances the possibility of carrying out structural analysis of ordered adsorption and epitaxial systems on surfaces. For these systems, the effects of multiple scattering can be often neglected, and geometric parameters can be estimated, as well as the type of the lattice formed by the adsorbed atoms and location of these atoms on the surface can be established.[28, 41, 61–64] Smekal *et al.*[65] considered the applicability of single scattering approximation to analysis of crystals with a high level of structure imperfection, polycrystalline and even amorphous materials. The single scattering approximation is efficient in the analysis of XPD patterns obtained after interference of backscattered electron waves which were emitted by adsorbate atoms on a surface. It is preferable for this purpose to observe XPD of photoelectrons with low kinetic energy. Such analysis of the $c(2\times2)$S/Ni(001) absorption system resulted in determination of geometric parameters of the surface structure, *viz.*, location (which is characterized by the z parameter) of the $c(2\times2)$S adsorbed layer on the Ni(001) single crystal surface and the first interlayer spacing (d_{12}) for the Ni(001) face.[66] Thus, the single scattering approximation operates well in the studies of processes occurring directly on surfaces when the model clusters describing the system are not large.

The results of investigation of ordering of endohedral fullerenes $Dy_3N@C_{80}$ on the Cu(111) surface can be cited as an example of modelling in the single electron scattering approximation.[67] The STM images of the $Dy_3N@C_{80}$/Cu(111) surface and the results of XPD analysis, including experimental patterns and modelling of electron photoemission from C and N 1s levels are shown in Fig. 13. Since carbon atoms form the fullerene cage, whereas the nitrogen atom is located at the centre of the system, the diffraction patterns reflect the view of fullerene from the outside or inside depending on the atom (C or N) chosen as the emitter. As the kinetic energy of photoelectrons is > 400 eV, the effects of forward scattering dominate in the diffraction patterns.

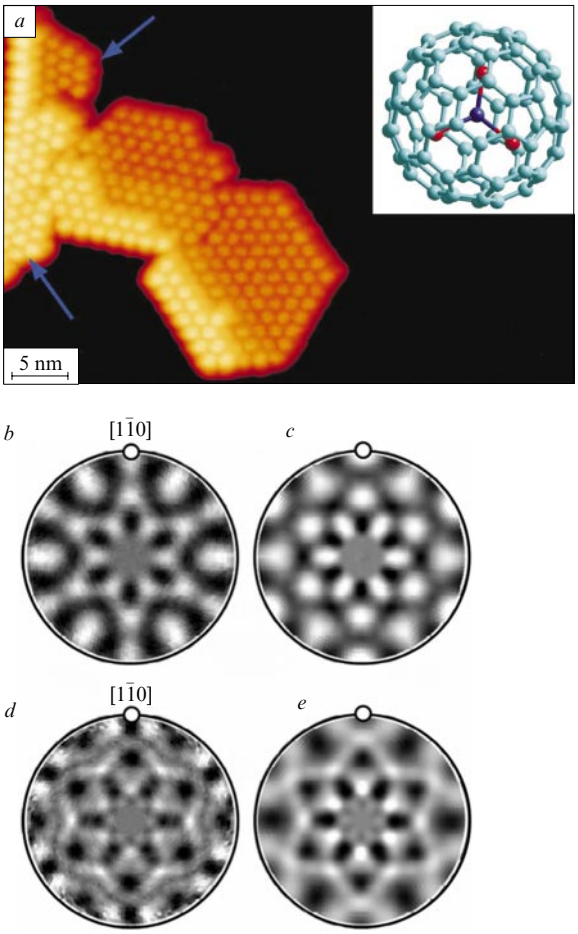


Figure 13. STM image of the surface of the $Dy_3N@C_{80}/Cu(111)$ system (the inset shows the model of endohedral fullerene) (*a*) and experimentally obtained 2π patterns of carbon (*b*) and nitrogen (*d*) 1s electron diffraction and corresponding simulated diffraction patterns (*c* and *e*) calculated in the approximation of single scattering of electrons.[67]

The fact that the XPD patterns for C1s and N1s photoelectrons are observable and have clear-cut scattering maxima indicates that the adsorbed fullerenes on the Cu(111) surface are ordered. From the results of calculations of the XPD patterns, which were carried out in the single scattering spherical wave approximation, a geometric model of the $Dy_3N@C_{80}/Cu(111)$ system was constructed, and interatomic distances in this model were determined.

In the case of more complex systems, it is desirable to use the multiple electron scattering approximation. Particularly, the effects of multiple scattering have to be taken into account while studying single crystal surfaces the XPD patterns of which are formed by photoemission from ten (and more) surface layers, while model clusters contain a set of atomic emitters and a few layers of scattering atoms. It was demonstrated in a series of seminal experimental and theoretical studies [37, 48, 68–71] that due to these effects, the intensity maxima of forward scattering by the emitter local environment atoms become substantially weaker, and additional fine structure appears in the diffraction pattern. The results of calculation of multiple scattering of Al2s electrons, which were carried out by means of separable Green's functions, are shown in Fig. 14.[48] As can be seen, the effects of multiple scattering already occur for two scattering atoms in the chain. It is believed that for a complete description of this effect, it is sufficient to consider 6–8 scattering events in the calculations.

The multiple scattering was taken into account in the XPD studies of epitaxial layers and adsorbed molecular structures. Taking the Cu(111),[72] $RhO_2/Rh(100)$,[73] $(1\times1)O/W(110)$[45] and 1T-TaS_2 (see Ref. 74) systems as examples, it was shown that the computational algorithms using multiple scattering approximation are preferable to attain precise geometric parameters for surface epitaxial and adsorption layers. Among many studies performed in this field in recent years, several studies [75–82] are of special interest for our consideration. Particularly, Atrei [75] demonstrated that the intensity of the silver $3d_{5/2}$ emission significantly decreases along the closely packed NiO(001) layers

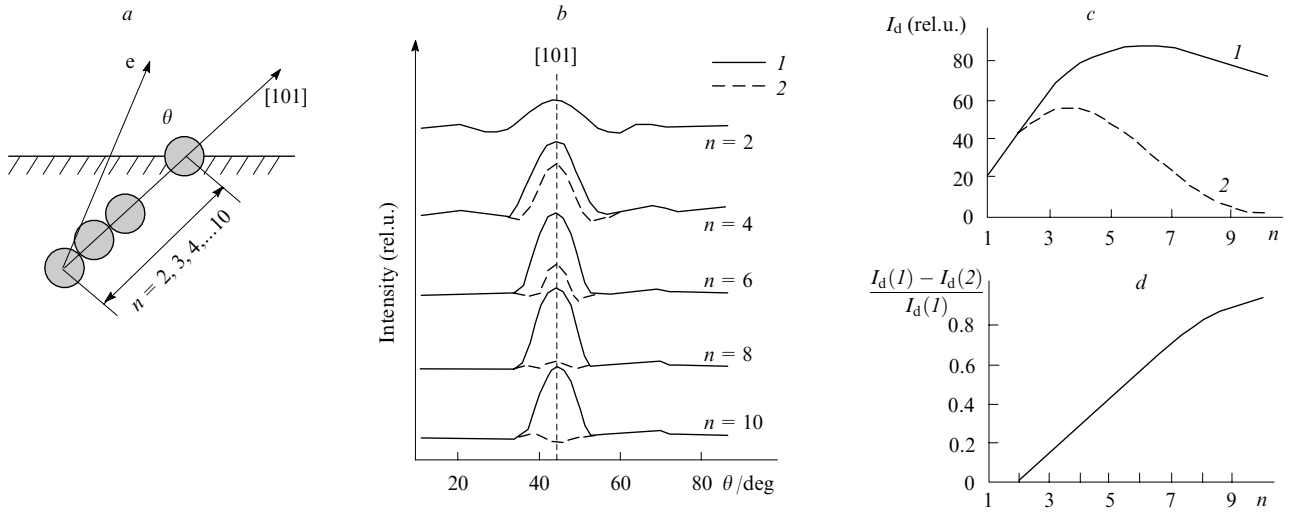


Figure 14. Results of calculation of single (*1*) and multiple (*2*) scattering in relation to Al2s photoelectron diffraction (E = 1336.0 eV) by a linear chain of aluminium atoms.[48]
(*a*) Schematic view of the location of the emitting atom; (*b*) calculated dependencees of photoemission intensity in models *1* and *2*; (*c*) scattering intensity in the Al[101] direction (I_d) *vs.* the number of aluminium atoms in the chain (n) in models *1* and *2*; (*d*) deviation of the results obtained with models *1* and *2 vs.* n.

deposited on the Ag(001) substrate. The analysis of epitaxial MnO films on the Ag(001) surface showed that for close-packed structures such as NaCl, the interpretation of XPD data in the framework of the forward scattering model is not sufficient.[76] When the multiple scattering model was applied, the precision of estimates increased 3–5-fold and tetragonal distortions were revealed for <5 nm thick film.[77] Network structures consisting of distorted MnO_6 tetrahedra were detected in the study[78] of epitaxial layers of $La_{0.7}X_{0.3}MnO$ (X = Ca, Sr, Ce) on $SrTiO_3$. It was found by means of analysis of diffraction of photoelectrons emitted by dopant atoms that the strontium and calcium atoms occupy definite sites in the crystal lattice, whereas cerium atoms are located arbitrarily.

In the case of unconventional surface systems, it may happen that the higher the quality of XPD simulation the more complicated is to bring the results into agreement with the experimental data. For example, it was impossible to determine the structure of TiO_2 clusters in an ultrafine TiO_2 film on the Pt(111) surface unambiguously from the XPD data.[79] Meanwhile, using calculations in the multiple scattering spherical wave approximation, which is sensitive to the local environment of the emitting atom, it was possible to detect dissolution of the ultrafine iron film deposited on the Ag(001) surface to a multitute of non-oriented clusters.[80]

Using the multiple scattering approach in the analysis of diffraction of photoelectrons emitted by oxygen 1s state and lead $4f_{7/2}$ state, Despont *et al.*[81] determined the direction of growth of the anisotropic ferroelectric $PbTiO_3$ film on the $Nb–SrTiO_3$ surface; it is virtually impossible to attain this result by any other methods at a film thickness of ~ 6 nm. A unique XPD experiment with resolution of carbon chemical states and calculations in the multiple scattering approximation demonstrated[82] that first two graphene monolayers epitaxially deposited on the 6H-SiC(0001) surface form a common buffer monolayer with a cellular structure.

Lately, owing to improvements in mathematical formalism of calculations in the multiple scattering spherical wave approximation, most of structural XPD studies have been carried out with the use of this approach. As an example, we mention the very good agreement between the results of calculations and experimental data shown in Fig. 11. Some discrepancies in the region of low kinetic energies of photoelectrons are rather related to the statistics of the experiment than to the accuracy of model calculations. A good compliance between experiment and theory is observed in the XPD patterns of the Cu(111) surface (see Fig. 3).[27] These experiments were carried out using a unique toroidal analyzer and the calculations were performed in the multiple scattering approximation.

In general, one can conclude that, at present, the technique of both XPD experiment and XPD modelling has reached high level. Of most popular programmes serving for XPD modelling, worth noting are EDAC[83] and MSCD (multiple scattering calculation of diffraction).[84] When model calculations are carried out using, for instance, the EDAC code, the following factors are taken into account: the geometry of the experiment, the type of polarization of synchrotron radiation, the size and shape of the modelled cluster, the number of scattering events to be taken into consideration, the electron mean free path in the material under study, the electron kinetic energy, and the energy level from which the electron is emitted. Additionally, such parameters as inner potential and the Debye temperature are used.[36]

Comparison of experimental and theoretical XPD patterns is carried out on the basis of *R*-factor: the smaller this factor, the better the agreement between theoretical and experimental data, and, hence, the more precise the description of the surface under study by the model cluster. The *R*-factor can be calculated in several ways. The following formula can be used for this purpose:

$$R = \frac{1}{n}\frac{\sum_n \sum_m |I^{\mathrm{exp}}_{n,m} - I^{\mathrm{th}}_{n,m}|}{\sum_m |I^{\mathrm{exp}}_{n,m}|} \qquad (6)$$

where n and m are the numbers of azimuthal and polar angle dependences, respectively; the superscripts exp and th stand for the experimental and theoretical values, respectively.[85]

The *R*-factor can also be calculated from the following equation:[66,86]

$$R' = \frac{\sum_n |\chi^{\mathrm{exp}}_n - \chi^{\mathrm{th}}_n|}{\sum_n |\chi^{\mathrm{exp}}_n|} \qquad (7)$$

Here, the normalized angular anisotropy is defined as follows:

$$\chi_n = \frac{|I^{\max}_n - I^{\min}_n|}{I^{\max}_n}$$

Finally, it was suggested[87] to determine the *R*-factor by the equation

$$R'' = \frac{\sum_n (\chi^{\mathrm{th}}_n - \chi^{\mathrm{exp}}_n)^2}{\sum_n \left[(\chi^{\mathrm{th}}_n)^2 + (\chi^{\mathrm{exp}}_n)^2\right]}$$

where

$$\chi(\theta, \varphi) = \frac{I(\theta, \varphi) - I_0(\theta)}{I_0(\theta)}$$

and

$$I_0(\theta) = \frac{1}{N}\sum_i^N (\theta, \varphi_i) \qquad (8)$$

Besides the above, other methods for calculating the *R*-factors have been suggested.[88,89] Any of the methods can be employed to compare experimental and theoretical XPD patterns, the choice being usually dictated by the methodological aspects of construction of the stereographic projections and the type of the problem to be solved.

The procedure for numerical estimation of goodness of fit between theoretical and experimental diffraction patterns brings XPD to a basically new level, namely, XPD can be considered as a method for structural analysis of surfaces. The use of *R*-factor forms the basis for optimization of geometric parameters of model clusters describing the surface or some structures on this surface.

This type of optimization can be exemplified by the results obtained in the study of the 1T-$TiSe_2$ crystal surface.[85] It is known that this crystal has a layered structure composed of three-layered Se–Ti–Se blocks separated by a van der Waals gap. The layered compounds (sulfides, selenides, tellurides) are convenient for experimental study as their crystals can be easily cleaved in vacuum along the

van der Waals gap to form structurally perfect and chemically clean surfaces. Many studies have been carried out using these objects, in particular, APRES experiments to investigate the band structure of compounds. However, the question of whether the structure of the crystal surface after the cleavage is the same as the bulk structure remains open.

STM and XPD experiments and quantum chemical calculations were carried out for the crystals of dichalcogenide 1T-$TiSe_2$.[90,91] The experimental and calculated diffraction 2π patterns for photoemission of Ti2p electrons and emission of Auger Se(LMM) electrons from the 1T-$TiSe_2$ surface are shown in Fig. 15 *a*. The calculations were done in the multiple electron scattering approximation considering the options of existence of structural defects in the 1T-$TiSe_2$ lattice, relaxation shrinkage (stretching) of surface layers and van der Waals gap and deviation of 1T-$TiSe_2$ surface geometry from the base (001) plane.

The EDAC programme using multiple scattering approximation for the chosen cluster[83] was employed for calculations. This programme is suitable for large clusters containing up to a few thousand atoms. Iterative procedures were applied to achieve fast convergence. The size and shape of the cluster are characterized by the quantity

$$R_{\max} \geqslant |r_i - r_0| + (z_{\text{surf}} - z_i)$$

Here, r_i and r_0 are the radius vectors to ith scattering atom and to emitter, respectively; z_{surf} and z_i are coordinates of the surface and ith scattering atom along the surface normal.

A parabolic-shaped cluster was used in this study;[83] its size was chosen to be approximately 1.5 times larger than the mean free path of an electron with energy of $\sim$1300 eV in $TiSe_2$ (Fig. 15 *b*). The number of atoms in the cluster was varied from $\sim$300 to $\sim$1000 depending on the location of the emitting atom relative to the crystal surface.

In the general case, matching theory and experiment requires a complex multiparametric analysis with optimization of geometry of the model cluster and search for the global minimum of *R*-factor. This is a very time-consuming task. In a simple embodiment, consideration can be restricted to several geometric parameters of the dichalcogenide crystal lattice, *e.g.*, one can vary the width of the van der Waals gap between the first and second Se–Ti–Se (*D*) blocks, interlayer relaxation inside the first upper block (*d*) and the lattice parameter *a* (see Fig. 15 *c*).[85] The crystal bulk parameters are used as the starting values, and then they are varied by being substantially increased or decreased. The diffraction pattern for Se(LMM) Auger electrons and *R*-factor for its divergence from experiment were calculated for each point of three parameters (altogether $>$500 points). As a result, *R*-factor quasi-surfaces for the set of the parameters *a* were constructed (Fig. 15 *d*).

The global minimum in the *R*-surfaces corresponds to the best coincidence of the experimental and theoretical XPD patterns and indicates the optimal parameters of the surface structure.[85] However, as can be seen from Fig. 15 *d*, there are two equivalent *R*-factor minima rather than one; therefore, the univocacy of the result has been questioned. The reason of this situation is the application of a simplified

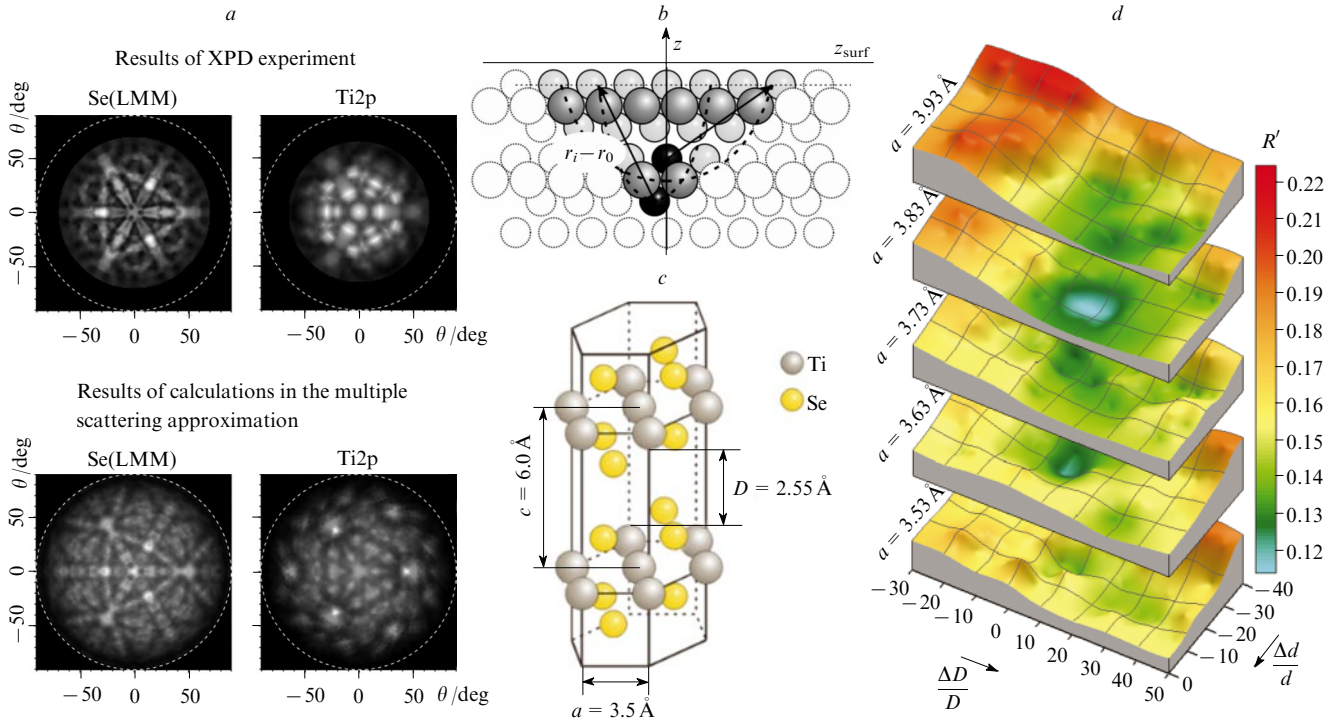


Figure 15. Results of XPD experiment and model calculations in the multiple scattering approximation for diffraction of Se(LMM) Auger electrons and Ti2p photoelectrons for the 1T-$TiSe_2$ surface (*a*), θ is the polar angle used to construct the diffraction patterns; divergence factor between theoretical and experimental XPD patterns (*b*); unit cell of the layered crystal of 1T-$TiSe_2$ with the indicated lattice parameters *a*, *c* and *D* (*c*); changes in the divergence factor surface depending on the deviations of the lattice parameters from their bulk values (*d*).[85]

model describing the surface. Both *R*-factor minima indicate significant deviation of the lattice parameters in the crystal surface layers from the corresponding bulk values. However, only linear distortions of the lattice were taken into account in the modelling, and the optimization was limited to three parameters. In view of the fact that a fairly simple model case of a pure single crystal surface was considered in this example, the question arises regarding the correctness of structure optimization on the basis of XPD data for more complex systems such as polyatomic molecules adsorbed on a surface and epitaxial layers, especially, if additional relaxation effects occur on the surface during adsorption or epitaxy.

Clearly, some initial information on the geometry of the scattering cluster is needed to solve the inverse problem of determining the surface structure from XPD data; this information is to be used for *R*-factor optimization, which is possible in the XPD method. This possibility is based on direct reconstruction of the scattering cluster structure from the XPD pattern using the holography formalism.

III. Photoelectron holography

The idea of visualization of atoms in a crystal lattice which underlies the atomic resolution microscopy (such as electron and scanning probe microscopies) cannot be completely implemented since two-dimensional projections of atomic structures are obtained by means of microscopy. Like photography, microscopy imprints the intensity of reflected (or transmitted, in the case of transmission microscopy) radiation. Similarly, only the amplitude (but not the phase) of the scattered wave can be recorded in the diffraction experiment, thus providing two-dimensional information about the structure of the reciprocal space. Only measurements of diffraction in all possible directions make it possible to reconstruct the crystal lattice. The direct visualization of three-dimensional atomic structure is a nontrivial task. For the first time, the idea of reconstruction of optical image of the atomic structure on the basis of diffraction data was expressed in 1920.[92] The development of the visualization concept in its final form belongs to Gabor,[93] who proposed in 1948 an original method for increasing the resolution of electron microscopes which was called holography (from the Greek *holos* meaning whole and *grapho* meaning to write).

The Gabor's method of visualization included two stages. At the first stage, the interference pattern of two electron beams, a reference beam not interacting with the substance and an object beam scattered by an atomic structure, was recorded on a multilayer photoplate. At the second stage, the obtained hologram was enlarged by a factor of a few thousand and irradiated with monochromatic radiation (whose wavelength was also increased by a factor of thousands relative to the electron beam wavelength). Owing to the light diffraction on the multilayer film, a detailed image of the three-dimensional crystal structure was formed. The development of lasers, coherent light sources, in the 1960s not only made it possible to fully implement the Gabor's concept in the field of atomic structure imaging but also made holography a popular technical and artistic means.

The principle of atomic holography was transferred to structural methods that use coherent radiation such as X-ray and neutron radiation or electron beam. The photoelectron holography technique is used to reproduce the atomic structure in three dimensions; therefore, the wave scattered by atomic structure plays the role of the object wave (ϕ_i). Usually, the same wave which has not undergone scattering serves as the reference wave (ϕ_0). The resulting interference of these waves contains holographic information.

At present, there are many options of atomic holography, and practically all of them are used to obtain structural information. Nevertheless, it is difficult to distinguish different types of atoms even upon detailed visualization. Photoelectron holography and related techniques, in which the chosen atom plays the role of the source of both object and reference waves of a photoelectron or an Auger electron, give a possibility to reconstruct the environment of the atoms of this type and also discern between the environments of the same atoms in different chemical states (Fig. 16).[94] This defines photoelectron holography as the only holographic method for gaining chemically meaningful information.

It is necessary to note that in the past few years, attosecond photoelectron holography has been actively developed; it is directed to imaging of ionization of atoms and molecules above their threshold under the influence of radiation of a high-power infrared free electron laser. As in the case of photoelectron holography, the source of both object and reference waves is the atom emitting a photoelectron. The holographic approach to the attosecond spectroscopy of xenon atoms has been reported in detail.[95] Below, we consider photoelectron holography based only on the data of photoelectron diffraction.

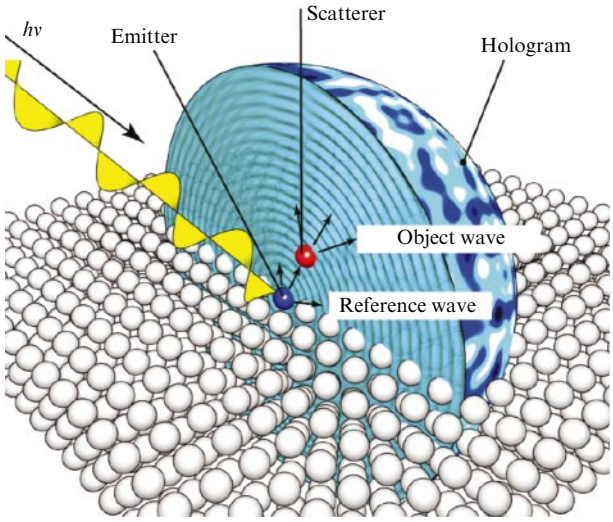


Figure 16. Schematic view of the formation of a photoelectron holographic image. The incident photon with the energy *hv* excites the emission of the electron wave outgoing from an atom on the surface (or in a subsurface layer) of a solid. The electron wave possessing a certain energy (wavelength) passes through the lattice above the emitting atom without scattering (the reference wave) and interferes with similar waves scattered by lattice atoms without energy loss (the object waves). As a result of the interference of the coherent waves, the holographic image of the local environment of the emitting atom is formed.[94]

Holographic images of argon and neon atoms were obtained using an atom that scattered incident radiation as a source of coherent radiation.[96] This study revealed the first problem of atomic holography with internal source: many identical sources create a great number of holograms, which are recorded simultaneously. Reconstruction of such a mixed hologram gives a mixed image of environments of all source atoms. It was a reason why most of holographic studies were carried out with single-element single crystals, whose atoms have equivalent positions and identical environment, and, therefore, their holograms coincide.

In 1986, it was suggested [23] to use atoms emitting photoelectrons as internal sources of radiation. Until that time, photoelectron diffraction patterns were not regarded as holographic because of the technical differences in information recording. Indeed, if an electron beam is used, a hologram is a result of single recording on a photoplate, the image can be then reconstructed with the use of an optical laser after enlargement of the record, whereas in the case of XPS, the diffraction pattern is an ordered set of a large number of spectral measurements; therefore, reconstruction of this hologram can be made by numerical processing of the spectra, but not by the optical method.

According to the idea of Szöke,[23] the subject of holography is the atomic environment of a point 'laser' generating the highly coherent reference wave. Therefore, the photoemission intensity $I(\boldsymbol{k})$ in Eqn (5) is described by a sum where the first term

$$\left|\phi_0(\hat{\varepsilon}\cdot\hat{\boldsymbol{k}})\right|^2 \equiv I_0(\boldsymbol{k})$$

characterizes the intensity of the reference wave, the second term

$$2\,Re\sum_i\left[\phi_0^*(k)\cdot\phi_i(k,r_i,\theta_{r_i}^{\boldsymbol{k}})\right]$$

is a result of the interference of the reference and object waves, while the third term

$$2\,Re\sum_{i\neq j}\left[\phi_i^*(k,r_i,\theta_{r_i}^{\boldsymbol{k}})\cdot\phi_j(k,r_j,\theta_{r_j}^{\boldsymbol{k}})\right]$$

describes the result of self-interference of the object waves. The holographic information is contained in the second term only. The third term can be neglected if

$$\left|\phi_0(k)\right| \gg \left|\phi_i(k,r_i,\theta_{r_i}^{\boldsymbol{k}})\right|$$

and then the hologram $\chi(\boldsymbol{k})$ is given by the equation

$$\chi(\boldsymbol{k}) = I(\boldsymbol{k}) - I_0(\boldsymbol{k}) \cong 2\,Re\sum_i\left[\phi_0^*(\boldsymbol{k})\cdot\phi_i(k,r_i,\theta_{r_i}^{\boldsymbol{k}})\right] \qquad (9)$$

In 1988, Barton [97] showed that the image of a surface structure can be obtained from the XPD pattern by means of two-dimensional fast Fourier transformation. The first reconstruction was carried out by Barton from the calculated pattern of diffraction of S1s photoelectrons for the $c(2\times2)$S/Ni(001) surface. The thus obtained image (Fig. 17) revealed high photoemission intensity near the actual positions of the atoms of the emitter local environment and made it possible to identify the site occupied by the adsorbate. However, the accuracy of coordinates of atoms surrounding the emitter was extremely low.

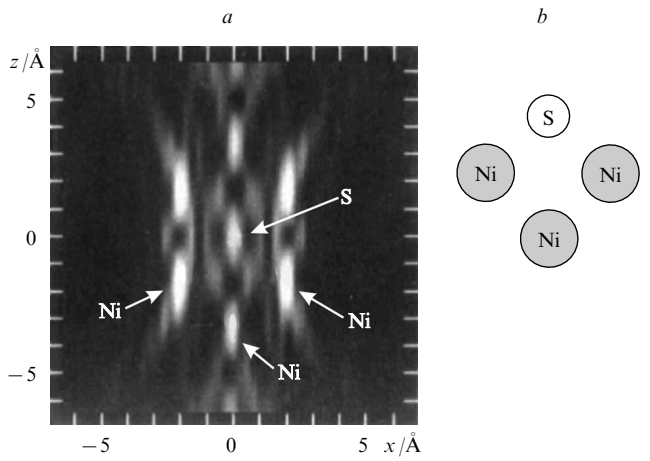


Figure 17. Cross-section of the holographic reconstruction obtained from the calculated S1s photoelectron diffraction pattern for the $c(2\times2)$S/Ni(001) surface in the plane perpendicular to this surface and passing through the emitter (*a*) and the model cluster (represented on the same scale) used in these calculations (*b*).[97]

Several algorithms based on correction of the anisotropy of the scattering factor were suggested to improve the accuracy of determination of the positions of atoms.[98–101] The disadvantage of this approach consists in that the peaks of forward scattering and diffraction rings bearing the information about the surface structure are partially overlapped, resulting in loss of a part of information about the atomic structure. Later on, the SWIFT (scattered wave included Fourier transform) algorithm was suggested,[102] taking into account the object wave anisotropy and the reference wave shape. This is especially important for Auger electron diffraction. An example of using the SWIFT integral for reconstruction of the structure of two-layered Cu(111) film is presented in Fig. 18.[99]

Barton [103] showed that the effects of multiple scattering, self-interference and coupling of holographic images can be substantially reduced if one uses a combination of holograms recorded at different kinetic energies. This approach provides a solution to the classical problem of coupling of holographic images, which was noted by Gabor back in his original work.[93] The necessity to subtract the reference wave from the XPD data gave rise to two main trends in

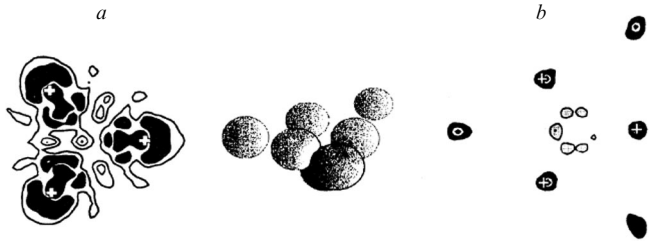


Figure 18. Images obtained after holographic reconstructions of the diffraction pattern on the surface of a Cu(111) two-layered film. The reconstructions were carried out using the simple Fourier integral (*a*) and the SWIFT integral (*b*). The crosses mark the exact atom positions. The structure at the centre represents the part of the cluster including the emitter and the upper layer of atoms.[99,102]

photoelectron holography, *viz.* near-node PH[99–102] and differential photoelectron holography[104–106] (DPH). Substantial contribution to the development and popularization of photoelectron holography as a research method was made by Fadley and co-workers.[107]

The recording of diffraction patterns near the nodal plane of the outgoing p-wave (near-node) was implemented by Wider *et al.*[104] In this case, the polarization vector of the incident radiation is practically perpendicular to the photoelectron emission direction, and, therefore, according to Eqn (2),

$$\left|\phi_0(\hat{\varepsilon}\cdot\hat{\boldsymbol{k}})\right|^2 \approx 0$$

as $\cos(\hat{\varepsilon}\cdot\hat{\boldsymbol{k}}) \approx 0$.

Due to the fact that photoelectron emitted from the s shell goes to a p orbital, scattering in the forward, side and back directions occurs more evenly in the case of the near-node approach as compared to other approaches. An example of application of the near-node technique to obtain photoelectron hologram of the Al(111) surface is shown in Fig. 19.[105] Two extreme alternatives are presented there; they correspond the near-node experiments at $\gamma = 0^\circ$ at which forward scattering towards the close packing of atoms is intensive, and at $\gamma = 80^\circ$ where the forward scattering intensity is minimized. The 3D reconstruction procedure was carried out based on the diffraction (holographic) patterns, and the result of significantly higher quality was obtained in the second case. The restrictions of near-node PH are associated with the necessity to have a source of synchrotron radiation and a special instrument and also with the objects of the study since it is preferable to deal with the emission from electron s levels. To date, the structures of the following systems have been studied by means of near-node PH: a pure Al(111) surface[105] and Cs–CO/Ru(0001) system containing a mixed adsorbed layer of caesium and CO on the ruthenium surface.[106]

Another approach[107, 108] to decreasing the contribution from forward scattering during the PH experiment was called differential photoelectron holography. It is based on the difference of two diffraction patterns obtained at close energies of incident radiation.

This approach implies replacement of the normalized intensity function χ [see Eqn (9)] by its derivative with respect to the photoelectron wave vector $\boldsymbol{k}$, or, more conveniently, by difference between the χ values obtained for two energies differing by a small quantity

$$\delta\chi = \chi(\boldsymbol{k} + \delta\kappa) - \chi(\boldsymbol{k})$$

With this approach, the effects of forward scattering can be substantially suppressed since

$$I_0\left[\hat{\boldsymbol{k}}(k+\delta k)\right] \cong I_0\left[\hat{\boldsymbol{k}}(k-\delta k)\right]$$

The DPH approach was applied to experimental and theoretical holograms of the Cu3p photoemission from the Cu(001) surface, the final 3D image proved to be of higher quality than the initial one.[107]

The differential photoelectron holography approach implies the following. The equation of hologram of single scattering for the emitter–scatterer pair located at the distance r is written as follows:

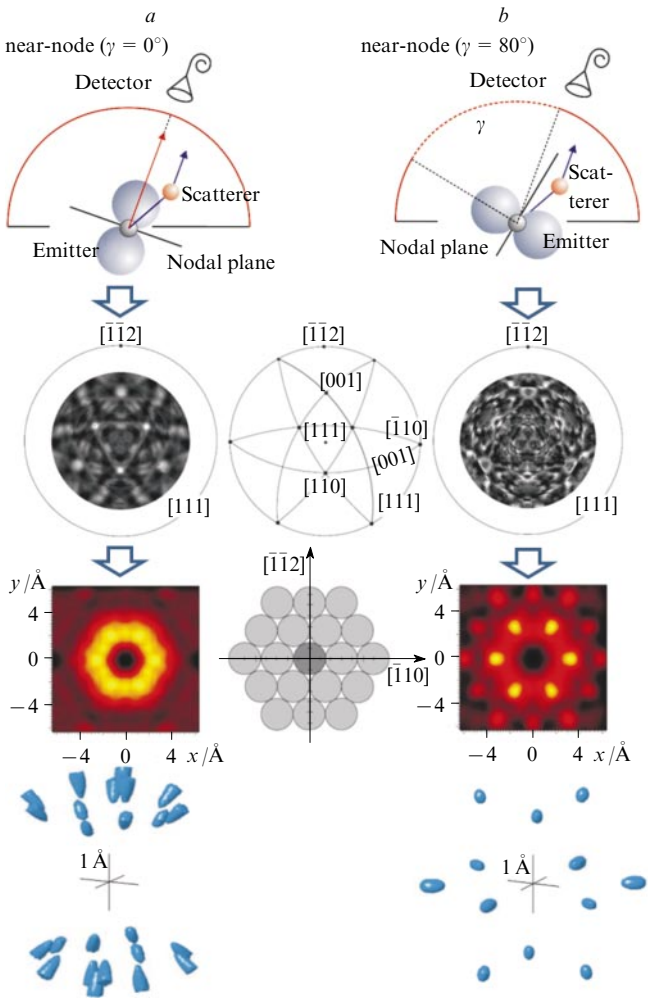


Figure 19. Formation of the three-dimensional image of the Al(111) surface using the near-node approach.[105]
Two versions of the experiments with the use of the near-node approach are shown, *viz.*, at $\gamma = 0^\circ$, the effects of forward scattering are dominant in the XPD pattern (hologram) (the second row on the left) (*a*) and at $\gamma = 80^\circ$, the effects of forward scattering are supressed (the second row, on the right) (*b*). The suppression of the forward scattering effects significantly improves the accuracy of the reconstruction of atomic structure of the surface as it seen from the shown cross sections (the third row) and 3D images (the fourth row) of the atomic structure of the Al(111) surface.

$$\chi(\boldsymbol{k}) = \frac{I - I_0}{I_0} \approx \frac{2\left|f(k,\theta_r^{\boldsymbol{k}})\right|}{r\cos\left[kr(1-\cos\theta_r^{\boldsymbol{k}}) + \psi(k,\theta_r^{\boldsymbol{k}})\right]}$$

where I_0 is the intensity without scattering by atoms, ψ is the scattering phase.[108]

If the quantity δk is small, so that

$$\frac{\delta|f|}{|f|} \ll 1$$

($\delta|f|$ is the change in the scattering amplitude $|f|$), then the difference between the two holograms for

$$k_\pm = k \pm \frac{\delta k}{2}$$

can be expressed by the following simple equation:

$$\delta\chi(\boldsymbol{k}) = \chi(k_+\hat{\boldsymbol{k}}) - \chi(k_-\hat{\boldsymbol{k}}) \approx \tag{10}$$

$$\approx -\frac{2|f_{\rm ef}|}{r}\sin\left[kr(1-\cos\theta_r^{\boldsymbol{k}}) + \bar{\psi}(k,\theta\boldsymbol{k}_r)\right]$$

where direction $\hat{\boldsymbol{k}}$ is determined by the θ and φ angles, $|f_{\rm ef}|$ is the effective scattering amplitude given by the formula

$$|f_{\rm ef}| = 2|f|\sin\left[\frac{\delta kr(1-\cos\theta_r^{\boldsymbol{k}})}{2} + \frac{\delta\psi}{2}\right]$$

$\bar{\psi}$ is the mean value of ψ for $k_\pm$. In the forward scattering region ($\theta_r^{\boldsymbol{k}} \to 0$), the $|f_{\rm ef}|$ value is small and in the limit $\delta\psi \to 0$ it approaches zero. If δk is also small, the $|f_{\rm ef}|$ quantity is proportional to r. Therefore, differential photoelectron holography makes it possible to reduce the forward scattering effects and, in addition, improve the quality of the images of atoms most remote from the emitter. However, the average value $\bar{\psi}$ still remains in Eqn (10), which may cause small shifts of atom positions in the 3D reconstructed image.[107]

What is the practical outcome of this approach? Two scattering amplitudes, the conventional ($|f|$) and effective DPH amplitute PH ($|f_{\rm ef}|$), are shown in Fig. 20 *a* as functions of the $\theta_r^{\boldsymbol{k}}$ angle for a pair of the closest neighbouring copper atoms spaced apart by 2.56 Å.[107] The photoelectron kinetic energy in this case is 295 eV.

It is clearly seen that the effective scattering amplitude loses its intensive maximum in the forward direction, somewhat increases in the backward direction and, what is important, becomes sensitive to the angle in the 30–90° region. At lower kinetic energies (for instance, as low as 81 eV used by Fadley *et al.*[107]), the effective scattering amplitude in the lateral directions decreases; therefore, it becomes difficult to detect an atom located in the angular sector of the forward scattering. The use of differential photoelectron holography is exemplified by the study of the Cu(001) surface (Fig. 20 *b*). As can be seen, the quality of the three-dimensional image is high. The emitting atom denoted by the letter 'e' is located in the zero-plane of the image, other atoms are below it and on the sides. Thus, the DPH technique reconstructs the atomic structure in the plane of the emitting atom and below it and, to a lesser extent, above it. It is suitable for studies of single-crystal surfaces. If adsorption of atoms or molecules on a surface is studied, apparently, an adsorbate atom should be chosen as an emitter. In this case, this atom and the substrate structure below it would be well identified.

Since the DPH experiment implies variation of the photoelectron kinetic energy, a source of synchrotron radiation is required, and this fact restricts the scope of application of DPH. The DPH experiments with Cu(100) and TiO_2(110) single crystals were performed using a laboratory spectrometer and a combined MgK_α (1253.6 eV) and AlK_α (1456.6 eV) anode.[109,110] From the diffraction patterns obtained for two kinetic energies of Cu3p photoelectrons, the difference hologram was constructed used for 3D reconstruction of the atomic structure. This approach does not quite meet the classical scheme of the DPH experiment, in which the photon energy changes only slightly. Nevertheless, such extention of the experimental base for photoelectron holography and, in particular, conducting experiments on laboratory equipment can only be welcomed.

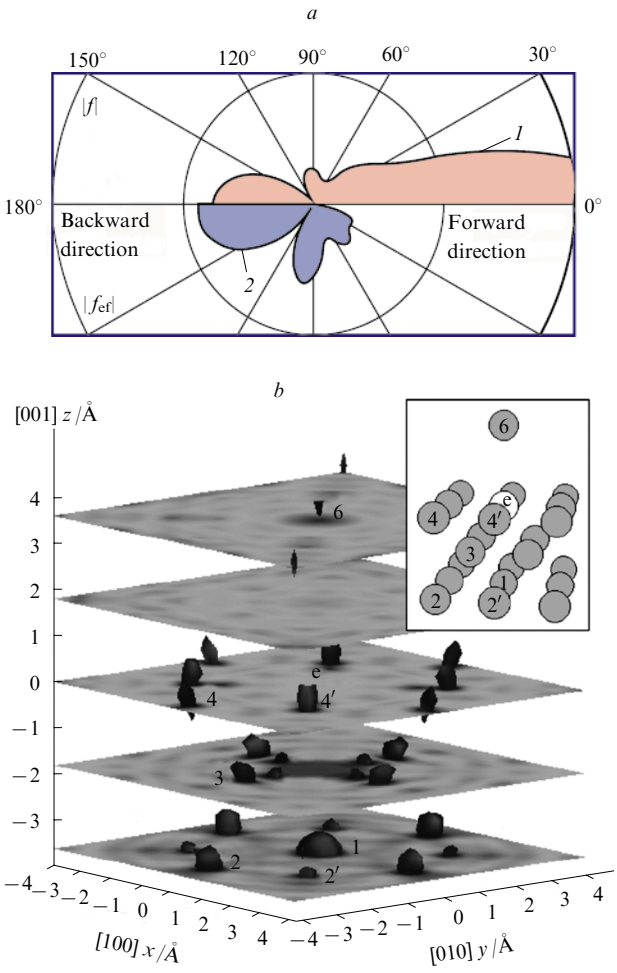


Figure 20. Angular dependences of the conventional (*1*) and 'effective' (for DPH) (*2*) amplitudes of electron wave scattering in the forward and backward directions (*a*) and 3D reconstruction of the atomic structure of the Cu(001) surface obtained using DPH (*b*).[107] (*a*) The Cu–Cu pair of atoms is chosen as an example, one atom emits the electron wave, the other scatters it; (*b*) the inset shows the model Cu(001) cluster with marked copper atoms playing the role of emitters (e) and scatterers (1–4) of electrons.

Other versions of photoelectron holography such as spin-polarized PH have been considered, and the effects of circular dichroism in PH have been discussed.[111–113] It is worth to note that there is a relatively new promising area in photoelectron holography, namely, the scattering pattern extraction algorithm with maximum entropy method (SPEA–MEM), which might become universal.

As indicated above, the reconstruction of 3D image from a photoelectron hologram according to the classical scheme [see Eqn (9)] is not accurate due to the effect of forward scattering and the phase shift in the region of forward scattering that impede the simple Fourier analysis. The reconstruction from a single energy hologram remains so far a rather difficult problem despite application of various methods for elimination of undesirable effects.

A Japanese research group suggested[24,94,114,115] a new fairly versatile algorithm, which is based on the application

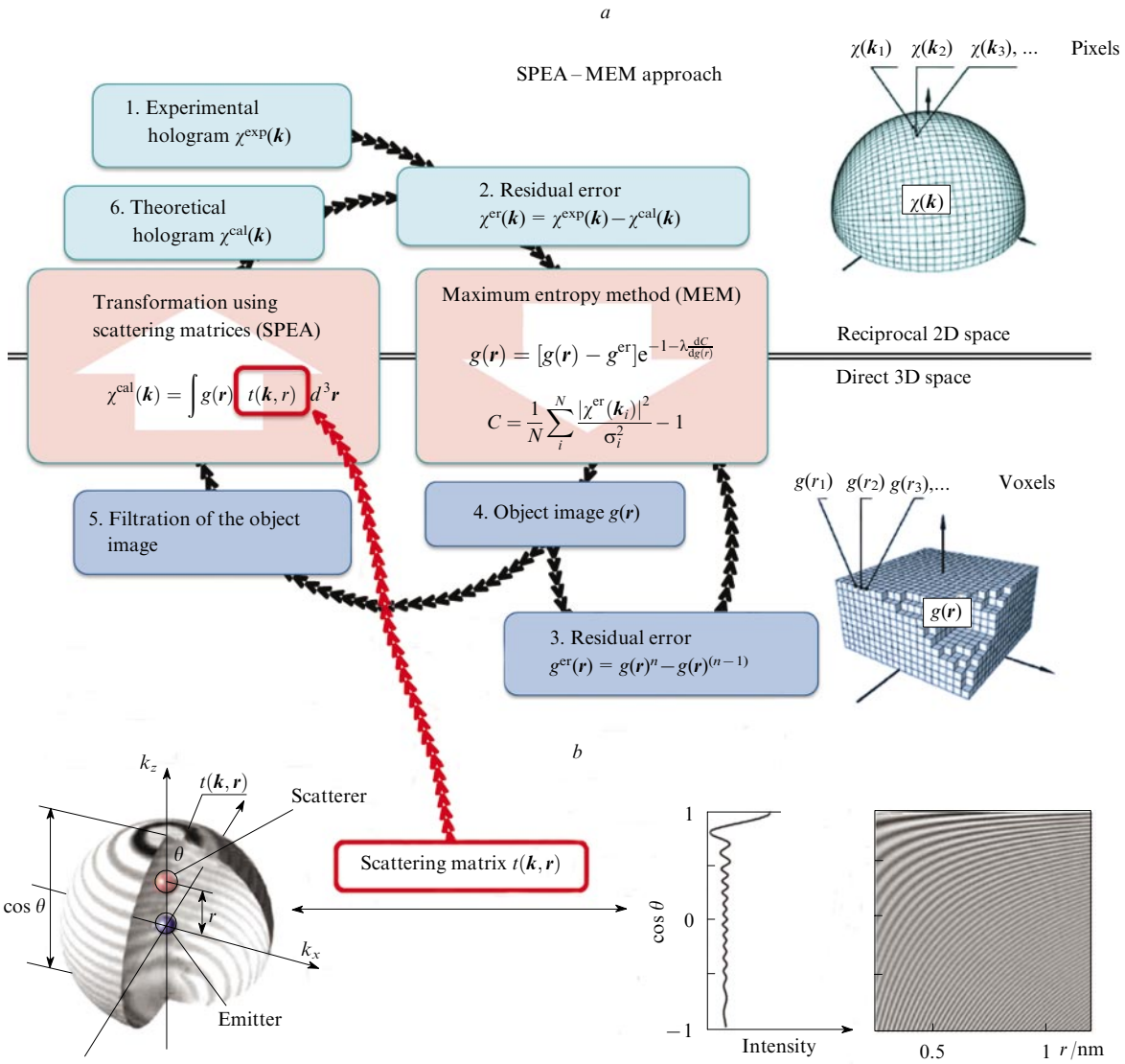


Figure 21. Schematic representation of the reconstruction of the 3D image of the atomic structure from XPD patterns using the SPEA – MEM approach.[24, 94, 115]

(*a*) The SPEA – MEM approach. 1. The starting data are represented by the experimentally obtained hologram $\chi^{exp}(\boldsymbol{k})$ in the two-dimensional reciprocal space (the XPD pattern). The starting values for the object (atom) image function in the real three-dimensional space $g(\boldsymbol{r})$ and the corresponding function of the computed hologram $\chi^{cal}(\boldsymbol{k})$ are specified. 2. The resdual systematic error $\chi^{er}(\boldsymbol{k})$ of the hologram calculation is determined. 3. The residual systematic error $g^{er}(\boldsymbol{r})$ in the real space is calculated. 4. The value of the function $g(\boldsymbol{r})$ of the object image is corrected by the parameters $\chi^{er}(\boldsymbol{k})$ and $g^{er}(\boldsymbol{r})$ using the maximum entropy method (MEM) (the equation is given in the Figure). 5. Filtration of the image and the operations of the translational symmetry are applied. 6. The object image is transformed into the theoretical hologram with the use of scattering matrices (SPEA), then the procedure starting from point 2 is repeated n times (n iterations) until the convergence of the solution with a given accuracy is achieved;

(*b*) Geometry of the function of electron scattering (E = 818 eV) by a copper atom. The relative positions of the emitter and scatterer and the hologram corresponding to this arrangement are shown on the left. From the location of the peak of forward scattering on the hologram, the direction from emitter to scatterer is determined, the distance r between these atoms can be obtained from the repetition rate of the diffraction rings. The information about the repetition rate of the diffraction rings can be reduced to the dependence of the intensity on the deviation angle θ. The set of these dependences for different values of the parameter r forms the scattering matrix.

of scattering matrices and the maximum entropy method and can be employed in the analysis of photoelectron holograms. The main advantage of this approach is the possibility of processing of a single hologram, and it is especially convenient in the case of the Auger holography.[114] This algorithm is based on the assumption that the reconstructed image is discontinuous. In other words, the perfect reconstruction should visualize the point positions of atoms, but not a continuous object. This assumption makes it possible to describe the scattering from each atom by a certain scattering matrix containing the information about the arrangement of interference rings at the specified angle relative to the line connecting the emitting and scattering atoms (Fig. 21). The scattering matrices can be computed by the SPEA program and are determined by the type of the scattering atom.[24]

The obvious fact of discontinuity of the atomic structure used in SPEA–MEM makes it possible to regard an XPD pattern as a hologram even if forward scattering maxima are present. If after conventional Fourier transformation of an XPD pattern, diffuse bands are observed in the forward scattering directions (see Fig. 17), in the case of discontinuity, atomic positions can be distinguished in these bands. The second assumption underlying this algorithm is that the atomic structure possesses the translational symmetry, which can be chosen to be three-dimensional or lateral.[115] This assumption results in intensification of the effects due to lateral scattering and thereby improves the reconstruction accuracy. The procedure of transformation from the reciprocal to direct space is based on the transformation of a two-dimensional element of XPD pattern (the hologram), a pixel, into three-dimensional element of the direct space, a voxel Fig. 21). The iterative maximum entropy procedure serves to attain the best correspondence of the experimental hologram (the XPD pattern) to the hologram calculated for the image reconstructed within the programme code.[94] The detailed description of SPEA–MEM and the fields of its application can be found in the publication of Matsushita *et al.*[24]

The SPEA–MEM approach is more friendly to the user than the earlier holographic approaches. At the same time, it is also not free from drawbacks. For instance, the artefacts in the form of unaccountable intensity maxima can appear in the 3D images of the atomic structure. Furthermore, if the atom under consideration has several non-equivalent positions in the lattice, the 3D reconstruction sums up the information about all of the positions, which greatly complicates the interpretation. In this case, it is helpful to compare the 3D reconstruction of the experimental hologram with a similar reconstruction of the XPD pattern computed for the model cluster. This approach makes it possible to label the artefacts in the 3D image and attribute the real maxima to the positions of certain atoms in the lattice. Available versions of this algorithm were tested in the studies of SiC,[116] $SrTiO_3$ (Ref. 117) and pure graphite surfaces,[118] and also of ultrafine films of iron silicide[119] and nano-sized films of silicon dioxide on a silicon substrate.[120]

Consider again the study of the 1T-$TiSe_2$ surface.[85] Recall that the result obtained by optimization of structural parameters of this surface with the use of *R*-factor was ambiguous since there were two global minima (instead of one) in the *R*-surface (see Fig. 15). Which of the two solutions is correct? The structure of atomic environments of the selenium and titanium atoms on the 1T-$TiSe_2$ surface was reconstructed using the SPEA–MEM technique, and the structural positions of the atoms were determined. It was found that the lattice of the diselenide surface layers was strongly distorted. Two upper Se–Ti–Se blocks (sandwiches) (~3.5 Å thick) are separated by a ~3.7 Å wide van der Waals gap, the parameter *a* being equal to ~3.85 Å. A shift of the titanium atoms along the [001] direction was revealed in the structural blocks on the crystal surface, the Ti layers are displaced by ~0.55 Å downwards

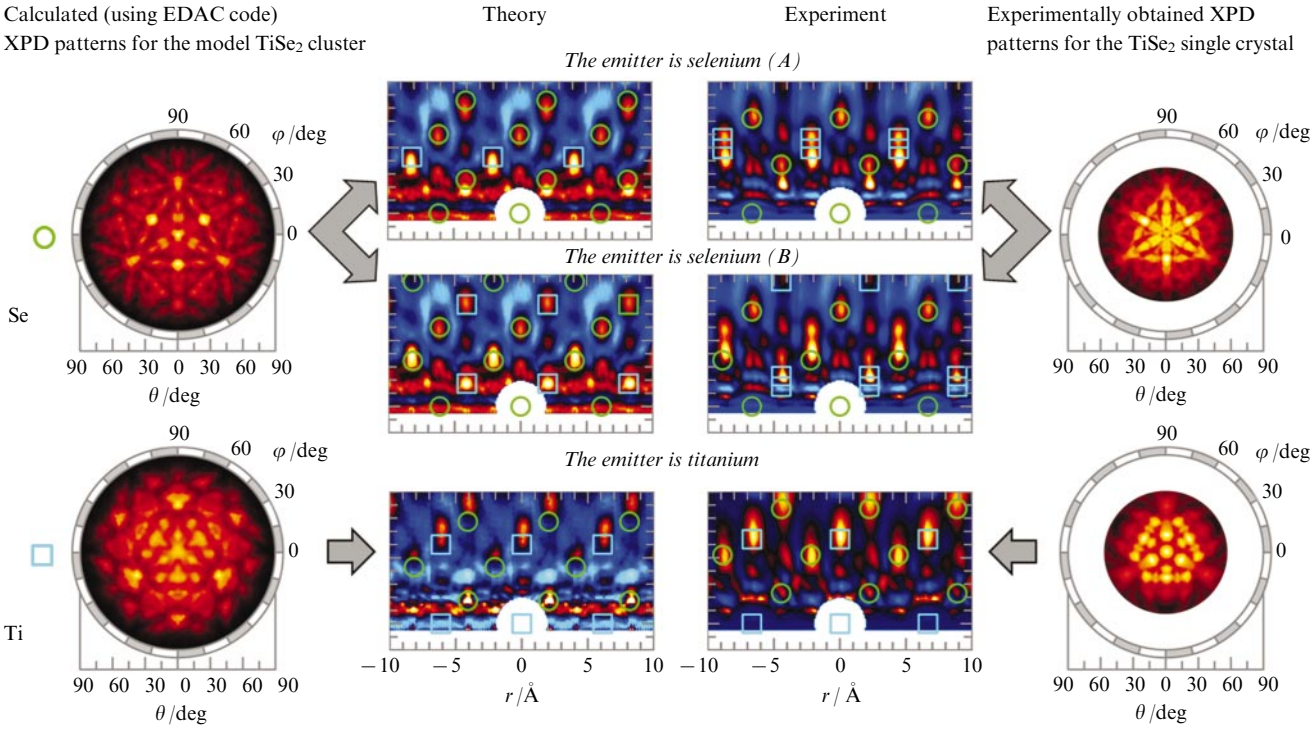


Figure 22. Results of analysis of the SPEA–MEM reconstruction of the XPD patterns for diffraction of Se(LMM) Auger electrons and Ti2p photoelectrons from the 1T-$TiSe_2$ surface.[121]
Theoretical and experimental XPD holograms for selenium (top) and titanium (bottom) are shown on the left and on the right, respectively. The cross sections in the (110) plane of the 3D image of the local environments of the selenium and titanium atoms in $TiSe_2$ are shown at the centre. The positions of selenium and titanium atoms are marked with circles and squares, respectively, *r* is the distance from the emitting atom.

in the upper block and by ~0.25 Å upwards in the second block. Thus, the holographic reconstruction gives the result similar to one of the solutions presented in Fig. 15 which corresponds to the *R*-factor minimum at $a = 3.83$ Å. Simultaneously, the 3D reconstruction predicts displacement of titanium layers in the Se–Ti–Se blocks, albeit with moderate accuracy; this possibility was not considered in the structural optimization with the use of *R*-factor. Therefore, the direct reconstruction is useful in the initial stage of analysis of XPD holograms, it should be followed by construction of a structural model and its subsequent *R*-factor optimization.

Nevertheless, the problems due to the imposition of 3D images from several non-equivalent positions of the atoms and appearance of artefacts after reconstruction remain. Both problems can be mitigated or even eliminated if, simultaneously with the reconstruction for the experimental holograms, the same procedure for the XPD images calculated for model clusters is carried out. An example for the case of the 1T-$TiSe_2$ surface is shown in Fig. 22.[121]

The fact that the crystal has a surface means that the system is asymmetric in the whole since there are the half-space containing the crystal material on one side of the surface, where the emission and scattering of electrons by the lattice atoms occur, and the half-space above the surface, where electrons move freely. Due to the non-equivalence of directions along one of the crystallographic axes, along the [001] axis in this case, the site symmetry of the emitting atoms is lower than their crystallographic site symmetry. As a result, there are two non-equivalent sites of selenium atoms in the layered 1T-$TiSe_2$ structure, corresponding to locations of the selenium atoms in the upper and lower layers of three-layered Se–Ti–Se blocks. Two upper blocks are analyzed. The titanium atoms are surrounded by selenium layers on both sides and, in the first approximation, all of them have the same crystallographic site. This is the reason why the 3D reconstruction for the titanium atoms is clear and unambiguous. On the contrary, in the case of selenium atoms, the 3D reconstruction includes information from two versions of their environment in the upper and lower layers, respectively. The model calculations of XPD followed by 3D structure reconstruction with the use of the SPEA–MEM method made it possible to exclude artefacts from the consideration and attribute the other maxima to the sites of titanium and selenium atoms in the 1T-$TiSe_2$ lattice.[85]

IV. Conclusion

This review is concerned with the development and the current state of a unique method for the analysis of surfaces — X-ray photoelectron diffraction. In the opinion of experts, over the past decades, XPD has transformed from a promising phenomenon into a reliable method for gaining structural and chemical information about surfaces. From the point of view of instrumentation, XPD is inseparable from such popular techniques as XPS and ARPES; together they constitute a line of related methods for thorough investigation of a surface at a depth of a few nanometres.

The distinctive features of XPD in comparison with other techniques of structural analysis such as LEED and STM are high chemical sensitivity to the surface conditions and a greater depth of analysis embracing ten (and more) surface layers. By chemical sensitivity we mean the ability to distinguish between different chemical forms of the chosen element (provided that the spectrometer resolution is sufficient) and to carry out the structural analysis for each form, but not merely the possibility to determine the type of an atom and the structure of its local environment. Mainly, two branches of XPD are developing actively:

— angle-scanned XPD, which is highly sensitive to the bond directions, and

— incident energy-scanned XPD, which is very convenient for determination of interatomic distances.

The former branch has been discussed in this review because angle-resolved XPD is more widely used since the experiments can be conducted using both laboratory spectrometers with light sources with fixed photon energy and synchrotron radiation with variable photon energy. In the case of energy-resolved XPD, a tunable radiation source is required, therefore the experiments can be carried out only at synchrotron centres.

In the case of angle-scanned XPD, 2π patterns in the form of stereographic projections result from the experiment. A separate 2π pattern is formed for each element on the surface or for its spectrally distinguished state. The type of the pattern reflects the structural position of the element, but strongly depends on different factors and, first of all, on the energy level from which the photoemission occurs and on the photoelectron kinetic energy. By varying these parameters, one can enhance or reduce the sensitivity of the method to the atomic environment above or below the emitting atom. As a result, XPD is adjustable to a particular task from the range of tasks spreading from the structural analysis of molecules adsorbed on surfaces to the study of layers under surfaces.

The XPD experiment can easily be implemented, resulting in 2π patterns with high angular resolution in a wide range of photon energies over a short period. To obtain the structural information from the experimental 2π patterns, it is necessary to solve the inverse or direct problem, thus reconstructing the 3D image of the local environment of the emitting atom. The structural analysis with the use of XPD has travelled a long way of development and currently, like its experiment technique, is at a very decent level of applicability. In some cases, the structures of molecules adsorbed on a surface can easily be understood from the angle-scanned XPD patterns without using numerical modelling. In more complicated cases, a detailed analysis of the data is required. For this purpose, the inverse problem is solved, *i.e.* theoretical calculations are carried out for different model clusters. The use of *R*-factor for comparison of experimental data with the results of modelling makes it possible to determine interatomic distances with accuracy within a few hundredths of angstrom. There are universal computer programmes (such as EDAC and MSCD) to calculate the intensities of photoelectron diffraction to a good accuracy.

In the case of even more complex systems, these approaches based on modelling do not lead to a positive result. At early stages of development of XPD, pure metal surfaces and adsorption of simple molecules were mainly studied. Later on, the compositions of single crystal surfaces and adsorbates became increasingly complex, and the interest switched to studies of subsurface layers and various ordered structures on the surface, relaxation effects, *etc.* This resulted in the situation when, having good experimen-

tal XPD data and possessing powerful software for their modelling, it was extremely difficult to carry out model computations and determine the surface structure due to the lack of basic information about the surface. Probably, this explains the slight decline of interest in XPD in the last decade. The active work in this field in the 1980s–1990s was aimed at understanding the XPD phenomenon and getting its mathematical description. Both tasks were generally solved. Therefore, one could expect wide application of XPD in various fields. However, the number of model tasks and simple systems is limited. In the case of more complex systems, many competing processes occur on surfaces, and non-obvious (at least at first glance) structures are formed. In this situation, it is extremely difficult to choose the suitable model cluster and optimize its parameters using the *R*-factor to control the convergence of theoretical and experimental XPD patterns.

This problem has been solved owing to development of photoelectron holography, which makes it possible to reconstruct the 3D space around the emitting atom and determine the positions of the atoms surrounding the emitter. The same diffraction 2π patterns play the role of the experimental basis of photoelectron holography; however, they are represented as holograms in this case. It is of special importance that the 3D reconstruction of atomic environment does not require any knowledge of the surface. The precision in determination of positions of atoms with the use of photoelectron holography is not high yet (the accuracy is ~ 0.2 Å in the best case), and subsequent conventional XPD calculations with the use of *R*-factor are necessary for accurate determination of the structure. The SPEA–MEM approach can be recommended as a numerical method for reconstruction of scattering cluster from XPD holograms.

In the whole, one can state that there is a powerful analytical method at the disposal of researchers, *viz*., X-ray photoelectron diffraction, which enables one to carry out a comprehensive analysis of the surface structure, including adsorption and epitaxial layers on the surface and layers that are few nanometres below the surface. It is very important that this method possesses well developed experimental and theoretical basis. In our opinion, the structural analysis should be started with the procedure of holographic reconstruction of the 3D structure of the scattering clusters around the emitting atoms of the elements contained in the surface. At the next stage, it is necessary to refine the structural parameters by means of model calculations of XPD and search for the minimum of *R*-factor, which reflects the degree of convergence of theoretical and experimental XPD patterns.

The review was prepared under financial support of the Russian Foundation for Basic Research (Project Nos 12-03-31030_mol-a, 11-03-00063-a and, 13-03-96032) and Ural Branch of RAS (Project No. 12-U-3-1006). The authors are grateful to E B Shalaeva and L V Yashina for useful discussion of photoelectron diffraction and holography data.

References

1. K Siegbahn, U Gelius, H Siegbahn, E Olson *Phys. Lett. A* **32** 221 (1970)
2. C S Fadley, S Ä L Bergström *Phys. Lett. A* **35** 375 (1971)
3. R J Baird, L F Wagner, C S Fadley *Phys. Rev. Lett.* **37** 111 (1976)
4. K Siegbahn, U Gelius, H Siegbahn, E Olso *Phys. Scr.* **1** 272 (1970)
5. F R McFeely, J Stohr, G Apai, P S Wehner, D A Shirley *Phys. Rev. B* **14** 3273 (1976)
6. R T Poole, R C G Leckey, J G Jenkin, J Liesegang *J. Electron Spectrosc. Relat. Phenom.* **1** 371 (1973)
7. J M Adams, S Evans, J M Thomas *J. Chem. Soc., Chem. Commun.* 210 (1978)
8. D P Woodruff *Appl. Phys. A: Mater. Sci. Proc.* **92** 439 (2008)
9. D A Duncan, W Unterberger, D Kreikemeyer-Lorenzo, D P Woodruff *J. Chem. Phys.* **135** 014704 (2011)
10. C S Fadley, M A Van Hove, Z Hussain, A P Ruebush *J. Electron Spectrosc. Relat. Phenom.* **75** 273 (1995)
11. M A Van Hove, C S Fadley *J. Phys. IV* **7** 65 (1997)
12. C S Fadley, S Thevuthasan, A P Kaduwela, C Westphal, Y J Kim, R Ynunza, P Len, E Tober, F Zhang, Z Wang, S Ruebush, A Budge, M A Van Hove *J. Electron Spectrosc. Relat. Phenom.* **68** 19 (1994)
13. A Tejeda, E G Michel *J. Phys.: Condens. Matter* **16** S3441 (2004)
14. G Faigel, G Bortel, C S Fadley, A S Simionovici, M Tegze *X-Ray Spectrom.* **36** 3 (2007)
15. C S Fadley *Surf. Sci. Rep.* **19** 231 (1993)
16. P Aebi, R Fasel, D Naumovic, J Hayoz, T Pillo, M Bovet, R G Agostino, L Patthey, L Schlapbach, F P Gil, H Berger, T J Kreutz, J Osterwalder *Surf. Sci.* **402–404** 614 (1998)
17. C S Fadley *J. Electron Spectrosc. Relat. Phenom.* **178–179** 2 (2010)
18. J Osterwalder, A Tamai, W Auwärter, M P Allan, T Greber *Chimia* **60** 795 (2006)
19. C Westphal *Surf. Sci. Rep.* **50** 1 (2003)
20. E V Shalaeva, M V Kuznetsov *Zh. Strukt. Khim.* **44** 518 (2003) [a]
21. D P Woodruff *J. Electron Spectrosc. Relat. Phenom.* **178–179** 186 (2010)
22. D P Woodruff *Surf. Sci. Rep.* **62** 1 (2007)
23. A Szöke, in *Short Wavelength Coherent Radiation: Generation and Applications (AIP Conference Proceedings N147)* (New York: American Institute of Physics, 1986) p. 361
24. T Matsushita, F Matsui, H Daimon, K Hayashi *J. Electron Spectrosc. Relat. Phenom.* **178–179** 195 (2010)
25. D P Woodruff, D Norman, B W Holland, N V Smith, H H Farrell, M M Traum *Phys. Rev. Lett.* **41** 1130 (1978)
26. M C Asensio *Surf. Rev. Lett.* **4** 295 (1997)
27. G P Cousland, A E Smith, J D Riley, A P J Stampfl *J. Appl. Phys.* **106** 093510 (2009)
28. A Fischer, R Fasel, J Osterwalder, A Krozer, L Schlapbach *Phys. Rev. Lett.* **70** 1493 (1993)
29. B Domenichini, G A Rizzi, P Kruger, M D Negra, Z Li, M Petukhov, G Granozzi, P J Mmller, S Bourgeois *Phys. Rev. B* **73** 245433 (2006)
30. B V Andryushechkin, K N Eltsov, V M Shevlyuga, C Tarducci, B Cortigiani, U Bardi, A Atrei *Surf. Sci.* **421** 27 (1999)
31. M V Kuznetsov, D P Frickel, E V Shalaeva, N I Medvedeva *J. Electron Spectrosc. Relat. Phenom.* **96** 29 (1998)
32. D P Frickel, M V Kuznetsov, E V Shalaeva *Surf. Rev. Lett.* **4** 1309 (1997)
33. R C G Leckey, J D Riley, A Stampfl *J. Electron Spectrosc. Relat. Phenom.* **52** 855 (1990)
34. F Matsui, T Matsushita, H Daimon *J. Electron Spectrosc. Relat. Phenom.* **178–179** 221 (2010)
35. H Daimon *Rev. Sci. Instrum.* **59** 545 (1988)
36. M A Matsushita, W H Weinberg, C-M Chan, in *Low-Energy Electron Diffraction* (Berlin: Springer, 1986) p. 603
37. M L Xu, J J Barton, M A Van Hove *Phys. Rev. B* **39** 8275 (1989)

38. A P Kaduwela, Ph.D. Thesis, University of Hawaii, Hawaii, 1991
39. M V Kuznetsov, E V Shalaeva, A G Panasko, M V Yakushev *Thin Solid Films* **451 – 452** 137 (2004)
40. E V Shalaeva, M V Kuznetsov *Fiz. Met. Metalloved.* **96** 45 (2003) [b]
41. R S Saiki, G S Herman, M Yamada, J Osterwalder, C S Fadley *Phys. Rev. Lett.* **63** 283 (1989)
42. A Sandell, A Nilsson, N Martensson *Surf. Sci. Lett.* **241** 1 (1991)
43. S A Chambers, S Thevuthasan, Y J Kim, G S Herman, Z Wang, E D Tober, R X Ynzunza, J Morrais, C H F Peden, K Ferris, C S Fadley *Chem. Phys.Lett.* **267** 51 (1997)
44. H Daimon, R Ynzunza, J Palomares, H Takabi, C S Fadley *Surf. Sci.* **408** 260 (1998)
45. F Matsui, M Fujikado *Czech. J. Phys.* **1** 61 (2006)
46. B R Cuenya, M Doi, S Lobus, R Courths, W Keune *Surf. Sci.* **493** 338 (2001)
47. Y Jugnett, G Grenet, N S Prakash, T M Due, H C Poon *Phys. Rev. B* **38** 5281 (1988)
48. A P Kaduwela, D J Friedman, C S Fadley *J. Electron Spectrosc. Relat. Phenom.* **57** 223 (1991)
49. D J Friedman, C S Fadley *J. Electron Spectrosc. Relat. Phenom.* **51** 689 (1990)
50. Y U Idserda, D E Ramaker *Phys. Rev. Lett.* **69** 1943 (1992)
51. A Winkelmann, C S Fadley, F J Garcia de Abajo *New J. Phys.* **10** 113002 (2008)
52. S Takahashi, S Kono, H Sakurai, T Sagawa *J. Phys. Soc. Jpn.* **51** 3296 (1982)
53. D Sebilleau, M C Desjonqueres, D Chauveau, C Guillot, J Lecante, G Treglia, D Spanjaard *Surf. Sci.* **185** 527 (1987)
54. D G Frank, N Batina, T Golden, F Lu, A T Hubbard *Science* **247** 182 (1990)
55. D G Frank, N Batina, J W McCargar, A T Hubbard *Langmuir* **5** 1141 (1989)
56. L E Klebanoff, D G Van Campen *Phys. Rev. Lett.* **69** 196 (1992)
57. J J Barton, D A Shirley *Phys. Rev. B* **32** 1906 (1985)
58. S Y Tong, W M Kang, D H Rosenblatt, J G Tobin, D A Shirley *Phys. Rev. B* **27** 4632 (1983)
59. J J Barton, S W Robey, D A Shirley *Phys. Rev. B* **34** 778 (1986)
60. J J Rehr, R G Albers *Phys. Rev. B* **41** 8139 (1990)
61. M Greif, L Castiglioni, A P Seitsonen, S Roth, J Osterwalder, M Hengsberger *Phys. Rev. B* **87** 085429 (2013)
62. M V Kuznetsov, A S Razinkin, E V Shalaeva *Zh. Strukt. Khim.* **50** 536 (2009) [a]
63. R Kosugi, S Sumitani, T Abukawa, Y Takakuwa, S Suzuki, S Sato, S Kono *Surf. Sci.* **412 – 413** 125 (1998)
64. J Wider, T Greber, E Wetli, T J Kreutz, P Schwaller, J Osterwalder *Surf. Sci.* **417** 301 (1998)
65. W Smekal, W S M Werner, C S Fadley, M A Van Hove *J. Electron Spectrosc. Relat. Phenom.* **137 – 140** 183 (2004)
66. R S Saiki, A P Kaduwela, Y J Kim, J Osterwalder, D J Friedman, C S Fadley, C R Brundle *Surf. Sci.* **282** 33 (1993)
67. M Treier, P Ruffieux, R Fasel, F Nolting, S Yang, L Dunsch, T Greber *Phys. Rev. B* **80** 081403 (2009)
68. G S Herman, S Thevuthasan, T T Tran, Y J Kim, C S Fadley *Phys. Rev. Lett.* **68** 650 (1992)
69. M L Xu, M A Van Hove *Surf. Sci.* **207** 215 (1989)
70. J Osterwalder, E A Stewart, D Cyr, C S Fadley, J Mustre de Leon, J J Rehr *Phys. Rev. B* **35** 9859 (1987)
71. J Osterwalder, A Stuck, D J Friedman, A Kaduwela, C S Fadley, J Mustre de Leon, J J Rehr *Phys. Scr.* **41** 990 (1990)
72. L Despont, D Naumovicr, F Clerc, C Koitzsch, M G Garnier, F J Garcia de Abajo, M A Van Hove, P Aebi *Surf. Sci.* **600** 380 (2006)
73. R R Zhan, E Vesselli, A Baraldi, S Lizzit, G Comelli *J. Chem. Phys.* **133** 214701 (2010)
74. L Despont, F Clerc, M G Garnier, H Berger, L Forro, P Aebi *Eur. Phys. J., B* **52** 421 (2006)
75. A Atrei *J. Electron Spectrosc. Relat. Phenom.* **185** 470 (2012)
76. A Chasse, Ch Langheinrich, F Müller, S Hüfner *Surf. Sci.* **602** 597 (2008)
77. A Chasse, Ch Langheinrich, M Nagel, T Chasse *Surf. Sci.* **605** 272 (2011)
78. C Raisch, C Langheinrich, R Werner, R Kleiner, D Koelle, M Glaser, T Chasse, A Chasse *J. Appl. Phys.* **113** 063511 (2013)
79. F Sedona, M Eusebio, G A Rizzi, G Granozzi, D Ostermann, K Schierbaum *Phys. Chem. Chem. Phys.* **7** 697 (2005)
80. S Terreni, A Cossaro, G Gonella, L Mattera, L Duo, F Ciccacci, D Cvetko, L Floreano, A Morgante, A Verdini, M Canepa *Phys. Rev. B* **70** 115420 (2004)
81. L Despont, C Lichtensteiger, F Clerc, M G Garnier, F J Garcia de Abajo, M A Van Hove, J M Triscone, P Aebi *Eur. Phys. J., B* **49** 141 (2006)
82. L H de Lima, A de Siervo, R Landers, G A Viana, A M B Goncalves, R G Lacerda, P Haeberle *Phys. Rev. B* **87** 081403 (2013)
83. F J Garcia de Abajo, M A Van Hove, C S Fadley *Phys. Rev. B* **63** 075404 (2001)
84. Y Chen, F J Garcia de Abajo, A Chasse, R X Ynzunza, A P Kaduwela, M A Van Hove, C S Fadley *Phys. Rev. B* **58** 13121 (1998)
85. M V Kuznetsov, I I Ogorodnikov, A S Vorokh, A S Rasinkin, A N Titov *Surf. Sci.* **606** 1760 (2012)
86. M A Van Hove, S Y Tong, M H Elconin *Surf. Sci.* **64** 85 (1977)
87. D P Woodruff, A R Gozalez-Elipe *Chem. Phys. Lett.* **199** 625 (1992)
88. J B Pendry *J. Phys. C* **13** 937 (1980)
89. R Fasel, A Aebi, J Osterwalder, L Schlapbach, R G Agostino, G Chiarelo *Phys. Rev. B* **50** 14516 (1994)
90. A N Titov, M V Kuznetsov, A S Razinkin *Fiz. Tv. Tela* **53** 1009 (2011) [c]
91. A S Razinkin, A N Enyashin, T V Kuznetsova, A N Titov, A L Ivanovskii *Zh. Strukt. Khim.* **51** 747 (2010) [a]
92. M Wolfke *Phys. Z.* **21** 495 (1920)
93. D Gabor *Nature (London)* **161** 777 (1948)
94. T Matsushita, F Matsui, H Daimon, K Hayashi *e-J. Surf. Sci. Nanotechnol.* **9** 153 (2011)
95. T Marchenko, Y Huismans, K J Schafer, M J J Vrakking *Phys. Rev. A* **84** 053427 (2011)
96. L S Bartell, C L Ritz *Science* **185** 1163 (1974)
97. J J Barton *Phys. Rev. Lett.* **61** 1356 (1988)
98. S Thevuthasen, G S Herman, A P Kaduwela, R S Saiki, Y J Kim, C S Fadley *Phys. Rev. Lett.* **67** 469 (1991)
99. S Hardcastle, Z-L Han, G R Harp, J Zhang, B L Chen, D K Saldin, B P Tonner *Surf. Sci.* **245** L190 (1991)
100. S Y Tong, C M Wei, T C Zhao, H Huang, H Li *Phys. Rev. Lett.* **66** 60 (1991)
101. B P Tonner, Z-L Han, G R Harp, D K Saldin *Phys. Rev. B* **43** 14423 (1991)
102. D K Saldin, G R Harp, B P Tonner *Phys. Rev. B* **45** 9629 (1992)
103. J J Barton *Phys. Rev. Lett.* **67** 3106 (1991)
104. J Wider, F Baumberger, M Sambi, R Gotter, A Verdini, F Bruno, D Cvetko, A Morgante, T Greber, J Osterwalder *Phys. Rev. Lett.* **86** 2337 (2001)
105. T Greber *J. Phys.: Condens. Matter* **13** 10561 (2001)
106. T Greber, J Osterwalder *Chem. Phys. Lett.* **256** 653 (1996)
107. C S Fadley, M A Van Hove, A Kaduwela, S Omori, L Zhao, S Marchesini *J. Phys.: Condens. Matter* **13** 10517 (2001)

108. S Omori, Y Nihei, E Rotenberg, J D Denlinger, S Marchesini, S D Kevan, B P Tonner, M A Van Hove, C S Fadley *Phys. Rev. Lett.* **88** 055504 (2002)
109. A Suzuki, A Hashimoto, M Nojima, M Owaria, Y Nihei *Surf. Interface Anal.* **40** 1627 (2008)
110. A Hashimoto, A Suzuki, Y Kisaka, S Miyasaka, M Nojima, M Owari, Y Nihei *Surf. Interface Anal.* **40** 1638 (2008)
111. H Daimon *Phys. Rev. Lett.* **86** 2034 (2001)
112. R X Ynzunza, H Daimon, F J Palomares, E D Tober, Z Wang, F J Garcia de Abajo, J Morais, R Denecke, J B Kortright, Z Hussain, M A Van Hove, C S Fadley *J. Electron Spectrosc. Relat. Phenom.* **106** 7 (2000)
113. A Oelsner, G Fecher *J. Electron Spectrosc. Relat. Phenom.* **101** – **103** 455 (1999)
114. T Matsushita, F Z Guo, F Matsui, Y Kato, H Daimon *Phys. Rev. B* **75** 085419 (2007)
115. T Matsushita, F Z Guo, M Suzuki, F Matsui, H Daimon, K Hayashi *Phys. Rev. B* **78** 144111 (2008)
116. F Matsui, N Nishikayama, H Matsui, K Goto, M Hashimoto, T Hatayama, T Matsushita, Y Kato, S Tanaka, H Daimon *J. Phys. Soc. Jpn.* **80** 013601 (2011)
117. A Uesaka, K Hayashi, T Matsushita, S Arai *Phys. Rev. Lett.* **107** 045502 (2011)
118. F Matsui, T Matsushita, H Daimon *J. Phys. Soc. Jpn.* **81** 114604 (2012)
119. K Kataoka, F Matsui, Y Kato, T Matsushita, K Hattori, H Daimon *Surf. Rev. Lett.* **13** 209 (2006)
120. I Pis, M Kobata, T Matsushita, H Nohira, K Kobayashi *Appl. Phys. Express* **3** 056701 (2010)
121. I I Ogorodnikov, A S Vorokh, A N Titov, M V Kuznetsov *Pis'ma Zh. Eksp. Teor. Fiz.* **95** 414 (2012) [d]

[a] — *J. Struct. Chem. (Engl. Transl.)*
[b] — *Phys. Met. Metallogr. (Engl. Transl.)*
[c] — *Phys. Solid State (Engl. Transl.)*
[d] — *J. Exp. Theor. Phys. Lett. (Engl. Transl.)*